NTNU

Norwegian University of
Science and Technology

Offshore-Grid

Matias Ebbe Theisen

Master of Energy Use and Energy Planning

Submission date: July 2011

Supervisor: Terje Gjengedal, ELKRAFT
Co-supervisor: Øyvind August Rui, Statnett
Trond Toftevaag, Sintef

Norwegian University of Science and Technology
Department of Electric Power Engineering

Project Definition

A directorate group lead by NVE published in October 2010 the report 'Havvind - Forslag til utredningsområder'. It highlights cites suitable for offshore wind farms on the Norwegian shelf. Two such areas are Southern North Sea I and II with an estimated capacity of 1000-1500MW and 1000-2000MW respectively. Both these areas are also close to oil and gas installations. To allow for an increased power trade with the continent the Norwegian TSO, Statnett, wish to build more HVDC interconnectors to the countries around the North Sea. Southern North Sea I and II happen to be placed along two such interconnections considered. One is supposed to go from Kvilldal in Norway to the east coast of England, the other from Tonstad to Germany.

A possibility is to combine the HVDC interconnectors and the establishment of the offshore wind farms as a step towards an integrated offshore transmission grid in the North Sea. The wind farms can be integrated into an offshore AC grid supplying the oil and gas installations in the area. To transport the access power to shore the offshore AC grid is connected to the two HVDC interconnectors. This is accomplished by building a bottom fixed offshore converter station at both wind farms. The offshore converter stations will be connected as a third terminal along each interconnector resulting in two three terminal HVDC grids.

- From the TSO's point of view the establishment of such a grid raises important challenges as regards to development of offshore grid codes. By system analysis important information and foresight into the challenges can be achieved. This master thesis is therefore to concentrate on the establishment of a simulation model of the proposed grid structure, and perform system analysis. This includes to establish a power system model of the offshore DC grid, include an equivalent system model of the onshore grid and to perform system studies on the integrated AC and DC power system.

The work is to be done in correlation with research on the topic performed by Statnett and Solvina.

Abstract

This thesis has been conducted in cooperation with the Norwegian transmission system operator, Statnett, and their research on two new interconnectors linking Norway to England and Germany. The work presented in this thesis has considered one of these interconnectors, with a third terminal connected offshore to allow for integration of offshore wind power and oil platforms, as shown in fig. 1.

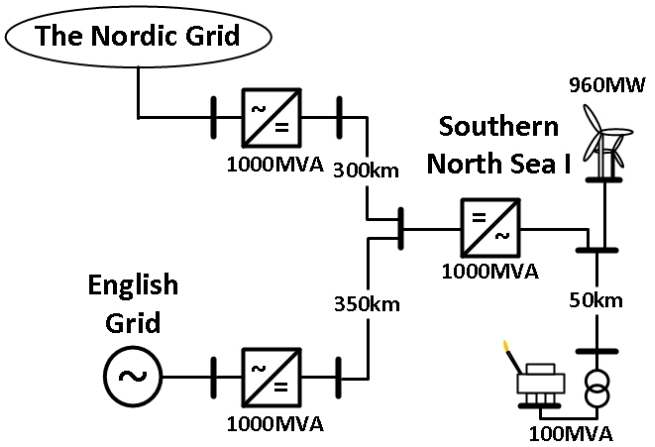

Figure 1: Schematic drawing of the three-terminal DC grid, used for the analyzes performed.

Investigation of the voltage source converters (VSCs) control ability as well as operational aspects of multi-terminal DC-grids has been performed. Identified as the key control variable of a DC-grid is the DC-voltage serving as a measure of power balance, since an unbalance will affect the DC-voltage through charging or discharging of the DC-capacitances. Utilizing VSCs allowing a fast and accurate control of the DC-voltage can lead to a stable operation of a DC-grid.

The three-terminal structure, fig. 1, was implemented in the simulation tool SIMPOW and connected to a 35-node AC-grid model representing the Nordic

grid. The simulation model was used for analyzes of the DC-grid operation and its affect on the connected AC-grids. The converter station connected to the Nordic grid were applied with DC-voltage control, implying that it will act as the power balancing unit of the DC-grid. The simulations performed show that the control structure implemented could assure a stable DC-grid operation within 0.3s of a fault. It identified the need for a fast response to changes in the DC-voltage as the influence of the other connected AC-grids were directly linked to DC-voltage oscillations.

Simulations were also conducted to study the advantage of applying AC-voltage control compared to reactive power for the converter connected to the Nordic grid. It was identified that an increased stability of the Nordic grid could be assured during faults in the grid itself. This also affected the DC-grid operation through an increased capability of power exchange with the Nordic grid.

Preface

Before presenting the thesis, I would like to thank all the people who have contributed and supported the work performed.

I want to thank Terje Gjengedal, my supervisor, for giving me the opportunity to write this thesis. The subject and the fact that the work has been related to ongoing research at Statnett has been a great motivation factor. I want to acknowledge the co workers of the research performed, Øyvind Rui from Statnett and Bengt Johansson from Solvina, for their discussions and contributions throughout the thesis. Special gratitudes are given to Trond Toftevaag from SINTEF for his endless support on all matters concerning the thesis. Further tanks are given to Lars Lindquist from STRI for technical support with SIMPOW.

The five years spent here at NTNU would not be the same without my friends. I would like to thank you all for the good times we have had together, making these years the best time of my life. Finally, I would like to thank my family for their endless love and support.

Contents

Chapter 1

Introduction

1.1 Motivation

There has been an increasing political drive for emission reduction by investments in renewable energy sources. Wind power is one of the most promising renewable power technologies, and especially offshore wind power benefiting from large areas with stronger and more constant wind. The European Wind Energy Association (EWEA) estimated in 2009 [1] that close to 50GW of offshore wind power will be installed in the European countries by 2020, increasing to as much as 150GW by 2030. The investments in offshore wind power is a major part of the European Union's 20/20/20-policy [2], and a contribution for making EU less dependent upon fossil fuel imports. Offshore wind power is also indicated by the Norwegian government to have a large potential. A directorate group has in this context presented a report [3] establishing suitable sites for offshore wind on the Norwegian shelf.

Due to the lack of storage capabilities wind turbines operate as to maximize the power output, giving a continuously changing production according to wind speed. This makes production planning a demanding task especially with the level of wind power proposed for the EU. The Norwegian hydro power has a high flexibility due to the capability for fast power ramping and energy storage in water reservoirs. This makes it compatible with the continuously changing wind power. Norway has therefore a large potential for deliver balancing power to

the European countries. In order to realize this potential new cable connections to the countries surrounding the North Sea are needed.

The new sites proposed for offshore wind farms in the North Sea tend to increase in size and distance from shore. High-voltage AC (HVAC) cables can only be used for a limited distance, due to high reactive power production of AC-cables. Therefore, high-voltage DC (HVDC) power transfer is seen as the more feasible solution for the new wind farm sites. With the amount of wind farms and international cable connections planned in the North Sea it is acknowledged in research [4], [5] that a multi-terminal DC (MTDC) grid would be a better solution compared to separate point-to-point connections. A MTDC grid will combine wind farms and international cable connections in an optimal way, limiting the number of cables and converter stations needed. Establishing offshore connection points close to offshore oil and gas installations additional emission reduction can be made by connecting the installations to the grid, shutting down the gas fired turbines they use for power production.

The realization of a MTDC grid is not a single application built in one stage. It needs a stepwise development integrating new wind farms and interconnectors as they are planned in the future. To accomplish this standardization must be agreed, allowing new technological solutions to be integrated in future expansions. Separate offshore grid codes need to be arranged, presenting criteria for connection. This will be a demanding task as there are several nations and companies operating with different framework and interests in the North Sea region.

As there are little practical experience with MTDC grids several perspectives need to be addressed. One of them being a control strategy for the grid operation. The grid needs a stable DC voltage even during large disturbances or faults. Since it is a desire to allow the connected converters to contribute with regulation on the AC side designated converters has to be equipped with DC-voltage control features. The control strategies has to be combined with fault detection and disconnection devices in order to give a high security of supply and degree of selectivity.

1.2 Scope and System Model

Statnett has acknowledged the potential of an offshore MTDC grid in the North Sea, and aims to have a vital role in its future development and operation. The company has taken an aggressive role towards research on the topic. This thesis is a part of the ongoing research work, and is in particular linked to work performed by the consultant company Solvina on behalf of Statnett. The aim for the joint research is to elaborate on the concept of an offshore grid. The research is performed in the view of a transmission system operator (TSO). Hence, no detailed analysis of separate grid components are done, but weight has been put on a complete system integration and operation. Identifying demanding operational aspects and dimensioning fault criteria is done and can act as a basis for the future establishment of offshore grid codes.

A specific grid structure has been proposed to serve as a basis for the research conducted,fig. 1.1(b), and is a possible first step towards a MTDC grid in the North Sea. The structure is based on two interconnections under consideration by Statnett, one to Germany and one to England. In addition two areas suitable for offshore wind power development [3] are near these interconnectors and can be integrated through establishment of offshore terminals. This part of the North Sea has also a considerable amount of oil and gas installations which is connected to the AC side of the offshore converter station. As can be seen in the fig. 1.1(b) the two offshore converters are interconnected on the AC side to allow for an increased security of power supply for the oil and gas installations.

As stated, several parties has taken part in the research. Therefore, a natural separation of the structure according to it's parts was performed. The work presented in this thesis considers mainly the two three-terminal DC grids, their operation and effect on the Nordic grid. As these are almost identical a model of one such three-terminal DC grid, shown in fig. 1.1(a), has been implemented and used for analysis in the simulation tool SIMPOW. This is the grid model referred to in further discussions, unless specified otherwise.

The second part of the complete grid structure is the offshore AC grid. The implementation and analysis of the AC grid is mainly performed by Solvina, presented in [6]. It has to be noticed that considerate amount of work has been done through this thesis on the offshore converter implementation and operation. The modeling of the two converter stations supplying the same AC grid and their regulation for power sharing were performed. As analysis of the

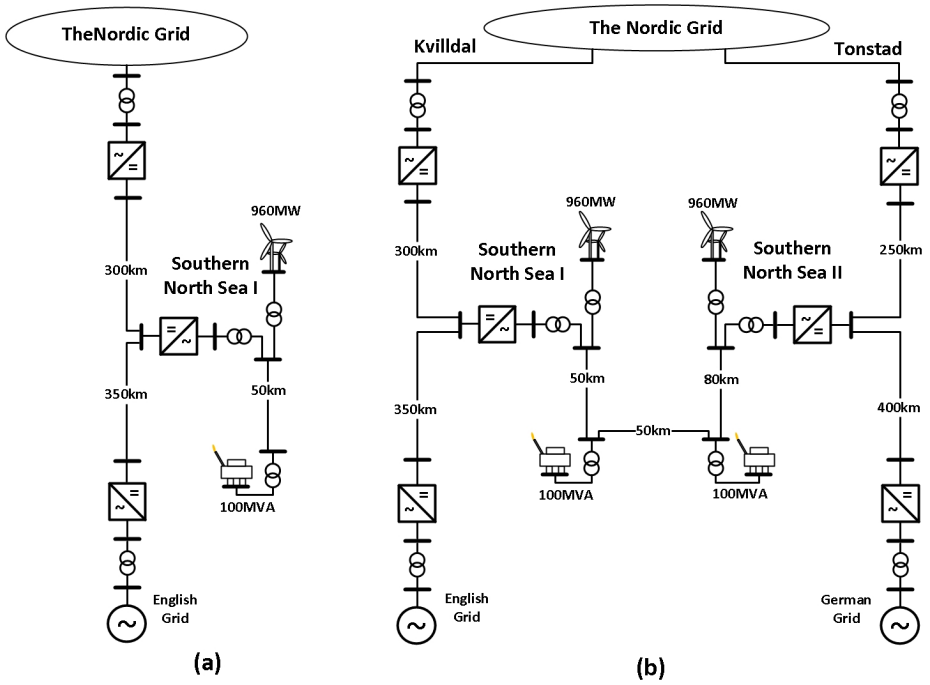

Figure 1.1: A three-terminal DC grid model used for the present work in this thesis (a); A schematic drawing showing the complete grid proposed (b).

offshore AC grid supplied by two converter stations where not a part of scope for this thesis no presentation of the models or their operation will be done.

The thesis investigates the following aspects:

- General technological development of power converters for use in HVDC grids.
- Converter control strategies for both AC and DC control features related to the proposed grid structure.
- Modeling of the grid structure in the simulation tool SIMPOW. Use of equivalent phasor based models offering the desired control features.
- MTDC grid operation and response to contingencies, analyzed through simulations. The converter control's affect on the connected AC grids and possibility for propagation of disturbances between the different AC grids connected to the MTDC grid.

1.3 Definitions

For further discussion the AC grids connected to the MTDC-grid are divided into three categories, according to their demand for converter control features.

- **Passive Grid** – A passive grid is a grid without any generation. It is therefore completely dependent upon its connection to keep a stable voltage and frequency. An example of such a grid, in the context of the thesis, is a connection of oil and gas installations without any wind farms or gas turbines.
- **Weak Grid** – A weak grid will have a certain amount of generation as for instance a combined grid with a wind farm and oil and gas installations. Although there are generation in the grid the connecting converter will need to offer control of active and reactive power to keep a stable frequency and voltage.
- **Stiff Grid** – A stiff, or strong, grid is a grid with a large amount of generation and loads. The grid will be able to keep a stable voltage and frequency irrespective of power output of the connecting converter. The onshore grid connections will be an example of a stiff grid.

To make discussions and explanations easier certain references for power flow, with regard to converter operation, are kept throughout the thesis.

- **Inverter mode** – The converter is supplying active power to the AC grid. It will therefore draw power from the DC grid to cover both the supply on the AC side as well as converter losses. However, the reactive power flow on the AC side, can be in either direction.
- **Rectifier mode** – The active power flow is turned, meaning that the converter is consuming power on the AC side to cover both losses and the supply on the DC side. As for the inverter mode, the reactive power flow can be in either direction.

Chapter 2

Converter Theory

In this chapter an introduction to the development of converter technology used for HVDC power transfer will be presented. The line-commutated converter will be compared with self-commutated converter. As this thesis considers converters for multi-terminal DC grids more weight will be put on the voltage source converter. Especially the modular-multilevel converter will be described in detail as this is the latest converter development, and the preferable choice in this context.

2.1 Line-Commutated Converter

The first DC-link [7] was put in operation, in 1954, between the Swedish mainland and the island Gotland. At that time, line-commutated converter's (LCC) based on mercury-valves were used. The thyristor-valve became commercially available in the late 1960's and is still the valve used for LCC's. Further development of the thyristor valves as well as the converter topology has pushed the HVDC-link power capability to the range of several GW with a DC voltage of up to ±800kV [8].

The high power rating together with the relative low losses is the dominating advantages of the LCC technology, but it comes with certain limitations and drawbacks. The thyristor-valves demand a strong synchronous grid voltage

in order to avoid commutation failures. That makes the LCC incapable of performing a black start of a grid and has restrictions when it comes to supplying weak grids.

As the commutation is done at a low frequency the LCC output voltage has a considerate amount of low frequency harmonics. The converters can only operate with a lagging power factor which implies a demand for reactive power. Both of these effects results in extensive filter components, increasing price as well as footprint of the converter station.

The LCC is also limited to two quadrant operation as the current can only flow in one direction. In order to change the direction of the power flow the voltage of the DC-link has to be reversed. In the context of MTDC grids this would imply extensive mechanical switch devices in order to allow separate power flow through each terminal. The voltage reversal also implies that extruded DC cables can't be utilized as it would result in charge accumulations leading to degradation of the cables [9].

Even with the aforementioned drawbacks HVDC-links with LCC is expected to be the dominating choice for bulk, point to point power transfer due to the high current, high voltage capability and low price of the thyristor-valves.

2.2 Self-Commutated Converter

A self-commutated converter, also known as voltage source converter (VSC), uses transistor instead of thyristors for valves. For high power applications insulated-gate bipolar transistors (IGBT) are the preferable choice today. As stated by the name, self-commutated, the transistors have the ability to switch both on and off, arbitrarily of current amplitude and direction. Not only can it switch on and off, but it does so at a incredible fast rate. It is due to this ability that the VSC does not share the same drawbacks as the LCC.

The fast switching of the valves means that the output voltage at the AC terminals can be modulated irregardless of DC voltage polarity. In addition, the current can flow in both directions leading to a controllable four quadrant operation. So in the context of MTDC grids the VSC is the preferable choice allowing each converter to control their power separately without any DC voltage reversal.

The four quadrant operation is also an advantage when supplying a weak grid. The converter can contribute with reactive power control increasing voltage stability. As the output AC voltage can be modulated by a virtual created reference the VSC can be utilized to supply passive grids and even perform black starts. The fast switching frequency creates only high order harmonics which reduces the need for filtering. As a consequence the VSC has a smaller footprint than the LCC.

Although, the VSC is superior to the LCC in many areas, it has some limitations. The IGBT has reduced current and voltage capabilities compared to the thyristor. Suppliers estimate that VSC with a power rating of 1,2GW and a DC voltage of ±500kV can be put in service with todays technology [10]. So compared with the LCC it is restricted in transfer capability. The high switching frequency of the transistors contribute to high losses, which is seen as one of the major drawbacks of the VSC. Other drawbacks like electromagnetic interference and increased transformer insulation stress are also primarily linked to the high switching frequency.

2.2.1 Two-Level Converter

A VSC can be built on many different converter topologies. However, most of the VSC in use for HVDC power transfer are built with a full-bridge, two-level topology. Figure 2.1 show a schematic drawing of the converter valve arrangement with three phase-units composed of an upper and lower valve. As stated by the name, the two-level converter switches the output voltage between two DC voltage levels.

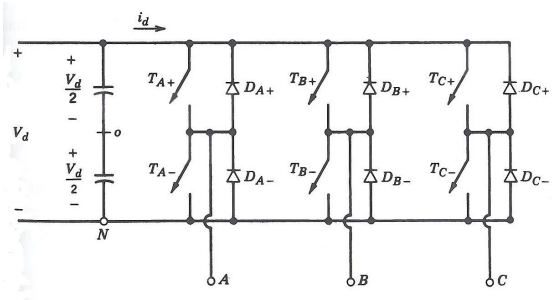

Figure 2.1: Schematic drawing of a full-bridge, two-level VSC converter [11].

The converters are typically controlled with a sinusoidal pulse-width modulation (SPWM). This results in a sinusoidal first-harmonic output voltage by comparing a rectangular carrier with a sinusoidal reference, as shown in fig. 2.2.

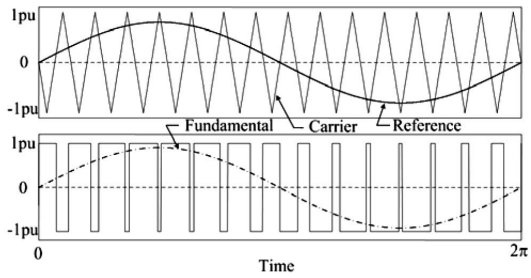

Figure 2.2: SPWM: Comparison of triangular carrier and sinusoidal reference, upper graph. Resultant phase voltage and first-harmonic, lower graph. [12]

The transistor has limited blocking voltage and current carrying capability. Therefore, several transistors are connected in series to increase the blocking voltage, and in parallel to increase the current carrying capability of the converter. During operation all these transistors have to be switched simultaneously to avoid uneven voltage and current distribution. For high voltage, high power applications like HVDC power transfer this can become a demanding task.

As stated in [12] a few three-level converters have been put in operation for HVDC power transfer. The topologies used in these are neutral-point clamped (NPC) and active neutral-point clamped (ANPC). The three-level topology implies that the output AC voltage is switched between three voltage levels. Therefore, less transistors are switched simultaneously thus reducing the switching losses. Also, due to the lower voltage steps a reduction in harmonic content and production of electromagnetic interference (EMI) is accomplished. For even better performance it has been a desire to increase the amount of voltage levels, but with the two topologies mentioned an even voltage distribution has shown to be difficult [12].

2.2.2 Modular Multi-Level Converter

The modular multi-level converter (MMC) is the latest development for HVDC-VSC. The first and only supplier to put an HVDC-link with MMCs in operation is Siemens for the Trans-Bay Cable Project, California [13]. Both Areva and ABB has followed by presenting their own modular multi-level converter topologies, [14] and [15].

As can be seen in fig 2.3(a) the MMC topology is similar to a full-bridge, two-level converter. The difference is that instead of a number of series connected transistors each phase-unit consist of series connected sub-modules. A sub-module is further built up by two transistors with a freewheeling diode and a capacitor, se fig. 2.3(b). By use of the two transistors, T1 and T2, the sub-

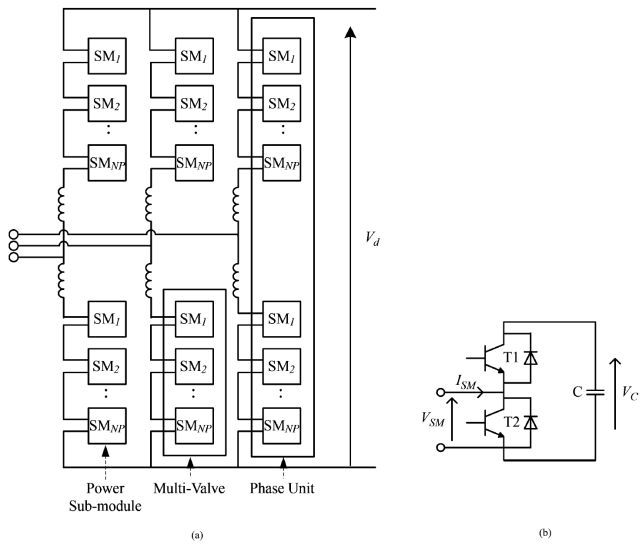

Figure 2.3: Schematic drawing of a MMC (a), and a sub-module (b). [12]

module can be switched between two operating states where current can flow in both directions. Table 2.1 show a summary of transistor state, output voltage and capacitor charging according to current direction. A state where both transistors are ON is never used as this will imply short circuiting the capacitor.

Sub-module state	**T1**	**T2**	I_{SM}	V_{SM}	**Sub-Module Capacitor**
ON	ON	OFF	> 0	V_C	Charging
ON	ON	OFF	< 0	V_C	Discharging
OFF	OFF	ON	> 0	0	No charging
OFF	OFF	ON	< 0	0	No charging
ON	OFF	OFF	> 0	V_C	Charging
OFF	OFF	OFF	< 0	0	No charging

Table 2.1: Possible states of an MMC sub-module

The principal operation of the MMC is explained by considering one of the three phase-units. As shown in fig. 2.3(a) each phase-unit consist of two multi-valves with NP number sub-modules. The two multi-valves are referred to as the upper and lower valve. Connected between the two valves is the AC voltage terminal of the phase-unit, also called the midpoint voltage. For simplicity it is assumed that the capacitor voltage is constant, $V_C = k$, so charging or discharging conditions are not considered. Upper and lower DC terminal in fig. 2.3 is the positive and negative DC voltage, respectively, with a voltage between them equal to V_d.

Let's assume that all sub-modules in the lower valve are ON and all in the upper valve are OFF. In this state the midpoint voltage will be equal to the positive DC voltage, and the total DC voltage will lie across the lower valve. Hence, the capacitor voltage can be described with (2.1)

$$V_C = k = \frac{V_d}{NP} \tag{2.1}$$

By changing the state of SM1 in both valves there are still NP sub-module in the ON state with a total voltage across the phase-unit equal to $NP * k = V_d$. The difference is that the midpoint voltage is moved with a step, $\Delta V = k$, towards the negative DC voltage. In this fashion a sub-module in each valve can be switched until NP voltage steps are completed, and the midpoint voltage is equal to the negative DC terminal voltage.

With the proper control of the sub-module switching the midpoint voltage can be made to follow a sinusoid in a stepwise manner. This is shown in fig. 2.4 for a phase-unit with twelve sub-modules in each valve.

As shown in tab. 2.1 the capacitors are either charged or discharged when connected. The result is a change in capacitor voltage, V_C. For proper operation it

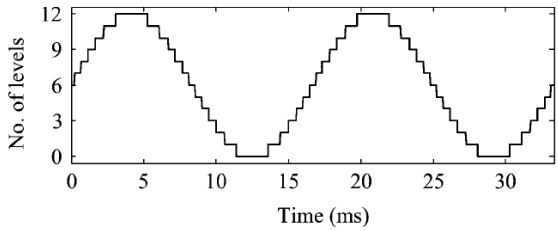

Figure 2.4: Output voltage curve over time in a twelve level modular converter [12]

is a necessity to keep the fluctuations in V_C at a minimum. This can be accomplished by over dimensioning the capacitors, but that would imply extra costs. To minimize the over dimensioning, capacitor voltage is measured allowing the control to switch the sub-module most suited during charging and discharging conditions. This way the voltage fluctuations are minimized and an optimal capacitor size can be chosen.

Comparing fig. 2.4 with the two-level output in fig. 2.2 it is easy to see that the MMC has considerable lower harmonic content and will produce less EMI. It is stated in [16] and [17] that the AC filters can be considerable reduced and even omitted for converters with more than 200 sub-modules in each valve. Also stated [15], is that no common DC capacitor is needed for the MMC, but a series rector in each valve. The series rector is needed to limit circulating currents and fault currents.

Although the filters are reduced, the MMC topology has a higher amount of components resulting in a more complex design. The amount of transistors needed is at least twice compared to a two-level converter. As the IGBT has a failure rate several orders higher than passive components this would be expected to give reduced reliability for the MMC. However, the modular construction offers a good solution. The modules are equipped with protective switches which shortcircuit the module if a IGBT fails. The result is only a marginal increase in voltage over the remaining modules and normal operation can be sustained. Even redundant sub-modules can be installed which are put in operation to replace the failed onces. The faulted sub-modules are then replaced during scheduled maintenance.

The major advantage of the MMC is the reduced switching losses. In the two-

level topology all series connected transistors in each valve are switched with a frequency of 1-2kHz. In the MMC each sub-module is switched only a few times during a period, leading to a total converter loss close to 1%. The effective switching frequency of the MMC is however not reduced and can be several orders higher compared to the two-level converter [15]. Hence, the MMC does not suffer in regulation responstime or fault handling capabilies.

Chapter 3

Control Abilities of VSCs

This chapter will address the possibilities of control when utilizing converters. It will concentrate on use of VSC as these are the preferable choice for MTDC grids.

In literature, the control features of the VSC is usually described using decoupling in a rotating dq-axis frame. This results in a separate control of active and reactive power. However, the implementations and analysis performed in SIMPOW is based on phasor representations. Therefore a review of a phasor based converter model and regulation, as it is implemented in SIMPOW, will be presented.

3.1 Phasor Model of VSC

In the context of HVDC power transfer the VSC serves as a link between the HVDC grid and a connected AC grid. It has been shown in research and applications that both the two-level [11], [18] and multi-level [17] VSC can offer a controllable link between the AC and DC side. When considering the first harmonic on the AC side and average values on the DC side an equivalent phasor model of the link will be as in fig. 3.1. In the figure the converter is operating in inverter mode, delivering active power to the AC grid. The nodes AC1 and DC1 is the AC and DC terminals of the VSC, respectively. The connection to

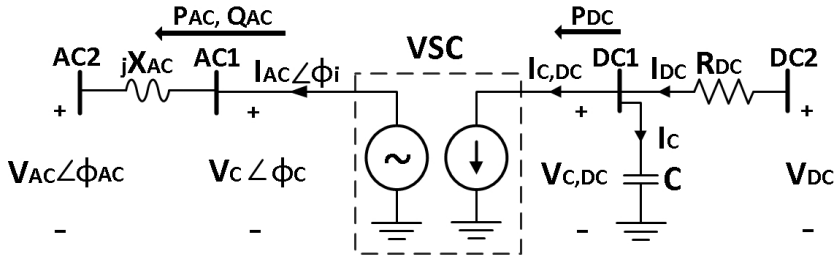

Figure 3.1: Equivalent model of a VSC

the AC grid (AC2) is through a reactance X_{AC} representing the converter reactors and transformer short circuit reactance. The DC terminals is connected to a the DC grid (DC2) through a resistive element R_{DC} representing a cable connection. The converter DC-shunt and capacitance of the cable is represented by the aggregated capacitance, C.

On the AC side the model will act as controllable voltage source with a amplitude according to the voltage relation given in eq. (3.1).

$$V_C = \tau \frac{\sqrt{6}}{\pi} V_{C,DC} \tag{3.1}$$

The controllable parameters of a VSC is τ and ϕ_C. The amplitude modulation index, τ, is used to scale the amplitude of the output AC voltage. This is equivalent to adjusting the duty cycle in a two-level converter or the amount of sub-modules switched in the multi-level converter. With the given amplitude relation $\tau = 1$ will imply a PWM converter in square wave modulation [11]. The second parameter is the voltage angle, ϕ_C, which is controlled by applying the modulated voltage a shift compared to the measured grid voltage.

The influence on the DC side is done by adjusting the injected current $I_{C,DC}$ in order to satisfy the power balance equation, given in (3.2).

$$P_{DC} = U_{C,DC}\, I_{C,DC} = P_{AC} + P_{loss} \tag{3.2}$$

The internal switching and conduction losses of the converter is represented by P_{loss}. The losses are implemented as given in eq. (3.3), where RP and R are specified resistances. This result in a voltage dependent loss, no-load losses, and

a current dependent loss, load losses.

$$P_{loss} = \frac{V_C^2}{RP} + I_{AC}^2 R \tag{3.3}$$

The active and reactive power delivered by the VSC to the AC grid can be described by eq. (3.4) and (3.5), respectively.

$$P_{AC} = \frac{V_C \, sin(\phi_C - \phi_{AC})}{X_{AC}} V_{AC} \tag{3.4}$$

$$Q_{AC} = \frac{V_C \, cos(\phi_C - \phi_{AC}) - V_{AC}}{X_{AC}} V_{AC} \tag{3.5}$$

3.2 Implementation of the Regulation

In order to control the voltage angle, ϕ_C, it has to be related to a reference. This is done by applying a angle PI-regulator as shown in fig. 3.2. The regulator

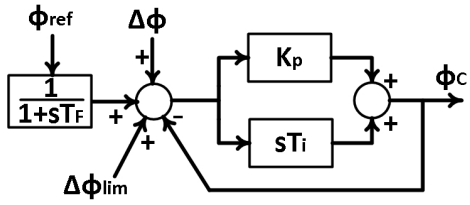

Figure 3.2: The converter angle PI-regulator

will force the voltage angle to equal the input values due to the feedback loop. A limit contribution is added, $\Delta\,\phi_{lim}$, to prevent high currents through the converter. Se sec. 3.2.1 for the implementation of the current limiter. The input $\Delta\,\phi$ is utilized to apply a desired shift compared to the reference angle. The low-pass filter is applied to represent the time delay of measurements.

The amplitude modulation index is also controlled with a PI-regulator, shown in fig. 3.3. The output is limited to keep the converter from going into over-modulation, resulting in high distortion and reduced control abilities. As for the angle regulator a limit contribution is added to prevent high currents. The input X_{meas} is a chosen parameter which is measured in the grid, typically this would

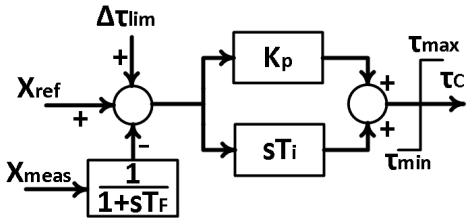

Figure 3.3: The converter voltage PI-regulator

be reactive power from the converter or voltage at a given node. It is passed through a low-pass filter to add the dynamics of measuring units. In order for the regulation to function, an increase in τ will have to increase the measured grid parameter. This will make X_{meas} serve as a feedback when compared to the desired reference value, X_{ref}.

3.2.1 Current limiter

To protect the VSC it is important to avoid currents and voltages above rated values. The current is therefore limited by use of a regulator as shown in fig. 3.4. The regulator is only active if the absolute value of the AC current crosses the

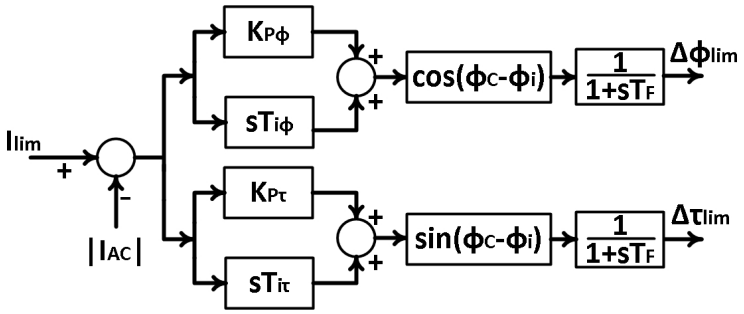

Figure 3.4: The converter current limit regulator

given limit, $|I_{AC}| \geq I_{lim}$. The output of the controller is weighted with the factors $sin(\phi_C - \phi_i)$ and $cos(\phi_C - \phi_i)$. This imply a reduction in angle if the active power through the converter is high, and a reduction in voltage amplitude

if the reactive power is high. A low-pass filter, with the time constant T_F, is added to simulate the time delay of the regulator response, which is primarily related to fault detection.

3.3 The Control Features

In literature, there are basically four different control features utilized to give the desirable behavior of a VSC, namely:

- Active power control
- Reactive power control
- AC voltage control
- DC voltage control

With the equivalent phasor model and the proposed regulation it can be shown that the same control abilities are attainable.

3.3.1 Active power control

When operating a MTDC grid it can be desirable to control the power output in a single terminal. This would be the case for the terminal in England in the proposed grid structure. By doing so the system operators can have complete control over the power exchange, giving a simple and predictable operation.

To accomplish this the reference angle for the regulator in fig. 3.2 is specified as the angle of the AC grid node (AC2). Then eq. (3.4) can be expressed as in eq. (3.6), where $\Delta\,\phi$ is the desired shift applied to the regulator.

$$P_{AC} = \frac{V_C\, sin(\Delta\,\phi)}{X_{AC}}\, V_{AC} \tag{3.6}$$

From this it is clear that the exchanged power is proportional to the controllable parameter $sin(\Delta\,\phi)$. Therefore, by applying a PI-regulator as in fig. 3.5, the shift in converter voltage angle can be adjusted as to keep the active power equal to a given reference.

Another form for active power control has to be applied when supplying a passive grid, or a weak grid where the VSC has to act as the balancing unit. This is the

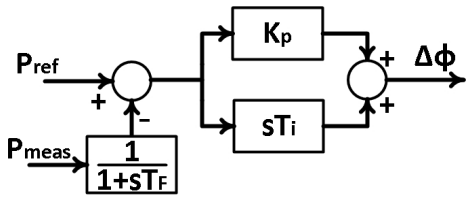

Figure 3.5: PI-regulator for control of active power

control feature applied for the offshore converter, Southern North Sea I. The offshore wind farms operate in a manner to maximize the power output and will therefore have a continuously varying power production. Therefore the VSC's has to adjust the power delivery in order to keep the balance in the grid.

For the phasor model this is accomplished by assigning a virtual angle reference, which is unaffected by the AC grid. The angle regulator in fig. 3.2 will than force the converter angle equal to this virtual reference. By assuming $\phi_{ref} = 0$ eq. (3.4) can be rewritten, eq. (3.7).

$$P_{AC} = \frac{V_C \, sin(-\phi_{AC})}{X_{AC}} V_{AC} \tag{3.7}$$

If the converter is operating in inverter mode $P_{AC} > 0$ and hence $-180\,^\circ < \phi_{AC} < 0$. An axcess of active power in the AC grid would lead to an increasing frequency. This will make $|\phi_{AC}|$ reduce in size compared to the unaffected reference. According to eq. (3.7) the delivered power to the grid will be reduced resulting in a new balance point. The opposite affect will happen in case of a power deficit. Hence, with the proposed control the VSC will act as a swingbus balancing the active power in the connected AC grid.

3.3.2 Reactive power control

The transfer of reactive power in an AC grid contributes to increased losses. It could therefore be desirable to utilize the four quadrant operation of the VSC to offer reactive power control. The reactive power could be set to a fixed value in order to give a certain degree of compensation, or set equal to zero minimizing the contribution from the VSC.

By combining eq. (3.1), (3.5) and the assumption that $cos(\phi_C - \phi_{AC}) \approx K$ the

reactive power delivered by the VSC can be described as in eq. (3.8).

$$Q_{AC} = \frac{\tau\, V_{C,DC}\, K - V_{AC}}{X_{AC}}\, V_{AC} \tag{3.8}$$

Assuming a constant DC voltage it is clear that an increased amplitude modulation index will lead to an increased delivery of reactive power.

To control the reactive power to be equal to a reference the PI-regulator shown in fig. 3.3 will be applied. The delivered reactive power will be measured and compared to a desired reference.

3.3.3 AC voltage control

To keep a stable voltage in the connected AC grid it could be desirable that the VSC contribute with AC voltage control. This is especially useful when supplying passive and weak grids as they are more vulnerable for voltage deviations during changed power conditions.

The voltage control could be applied to the converter AC terminals, which are directly proportional to τ. So by applying the PI-regulator in fig. 3.3 with the terminal voltage as the measured input, it would be regulated to follow a desired reference. In some situations however it is more desirable to control the voltage at an node elsewhere in the AC grid. As an example this could be the grid connection node (AC2) in fig. 3.1.

Lets assume the VSC is acting as the balancing unit in the AC grid, which imply that $\phi_C = 0$. The grid voltage can than be expressed by eq. (3.9).

$$\vec{V}_{AC} = V_C - j\, X_{AC} \vec{I}_{AC} \tag{3.9}$$

The current $\vec{I}_{AC}$ can be expressed by the delivered powers, eq. (3.10).

$$\vec{I}_{AC} = \frac{P_{AC} - j\, Q_{AC}}{\sqrt{3} V_C} \tag{3.10}$$

Combining (3.9) and (3.10) with (3.1) results in the following equation for the grid voltage, (3.11)

$$\vec{V}_{AC} = \tau\, V_{C,DC} - \frac{X_{AC}}{\tau\, \sqrt{3}\, V_{C,DC}} \left(Q_{AC} + j\, P_{AC}\right) \tag{3.11}$$

The voltage $\vec{V}_{AC}$ will have an increasing amplitude with increasing τ. Therefore by use of the PI-regulator in fig. 3.3 any desired node could be regulated according to a given reference. The node voltage needs to be measured to serve as a feedback to the regulator. It can be stated that if a node far from the converter terminal is chosen the feedback effect will be reduced resulting in poorly functioning regulation.

3.3.4 DC voltage control

As will be further discussed in Chapter 4 at least one converter in a MTDC grid needs to control the DC voltage. It is therefore of interest that the converter model can contribute with this control feature. To see how, it is assumed that the converter is in a stationary inverter mode of operation. A step in $\Delta\,\phi$ is applied resulting in an increased power delivery to the AC grid as shown in sec. 3.3.1. Through the power balance equation (3.2) this will be transferred to the DC side as an increased power demand.

The converter model apply the change in power demand as an increase in current, which can be described as in (3.12) by applying a deviation to the stationary DC current $I_{C,DC}$.

$$I^*_{C,DC} = I_{C,DC} + \Delta\, I_{C,DC} \tag{3.12}$$

According to (3.13) the current I_{DC} will not change as long as the DC voltages stay the same.

$$I_{DC} = \frac{U_{DC} - U_{C,DC}}{R_{DC}} \tag{3.13}$$

Hence, applying Kirchoff's current law to the converter DC terminal the relation between the change in current and DC voltage can be described by eq. (3.14).

$$\Delta\, I_{C,DC} = -I_C = -C\,\frac{dV_{C,DC}}{dt} \tag{3.14}$$

The sudden increased power demand will discharge the capacitor lowering the voltage at DC1, and therefore increase the current I_{DC}. A new stationary condition is accomplished where the increase in voltage angle, $\Delta\,\phi$ has resulted in a decrease in DC voltage. The DC voltage can therefore be controlled by adjusting the voltage angle, and hence power demand, accordingly.

This is accomplished by the use of the PI-regulator shown in fig. 3.6. Notice how the signs of the inputs are changed in order to get a reduction in $\Delta\phi$ if the measured DC voltage is lower than the reference.

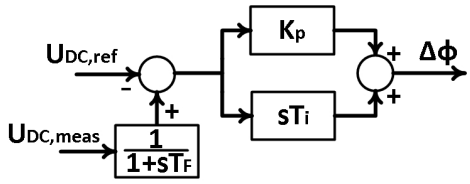

Figure 3.6: PI-regulator for control of DC voltage

Chapter 4

Multi-Terminal DC

This chapter will discuss the aspects of MTDC grids. Challenges related to operation and fault situations will be highlighted. Different research on the topic will be presented. All is viewed in the context of the proposed grid structure for this thesis.

4.1 Introduction to MTDC grid

With the introduction of converter technology and HVDC-links the idea of expanding to multi-terminal grids where soon studied. Already in the 1960's the basic construction and operation principals still in use today where suggested [19]. By the early 1990's four different projects where either in operation or under construction, all using LCC converters [20]. The larges project was the five terminal Québec–New England project [21], which has been reduced to a three terminal grid due to reliability considerations. From the 1990's all new HVDC power transfer projects has been constructed with point-to-point transmission.

Multi-terminal means that the grid has three or more connection point for power exchange. There are basically two different methods to build up a MTDC grid, namely series or parallel construction. The general structure of the two types can be seen in fig. 4.1. The series grid structure where studied as a solution

to the challenging task of power reversal in a parallel grid with LCC. With the series connection each terminal can change their power without affecting the operation of the others. However, this method demands that all converters conduct the full current in the connection lines, resulting in transfer capability restriction and high losses. Another disadvantage is if a converter fails the whole grid gets affected. All MTDC grids constructed has been built on the parallel structure. With the introduction of VSC capable of four quadrant operation it is doubtful that the series structure will be utilized in future projects.

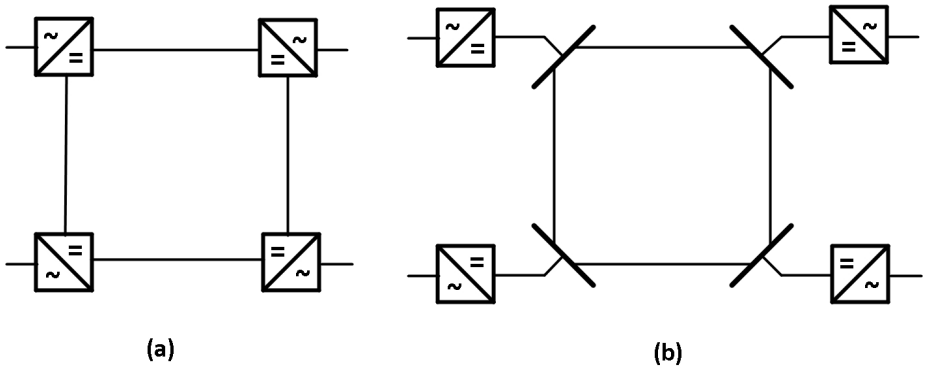

Figure 4.1: MTDC grid structures: Series connected(a); Parallel connected(b)

The main advantage of MTDC or DC transfer as such is the low losses, allowing long distance transfer of high power. The distance limitation of AC becomes even more evident in cable applications due to high reactive power production. Hence, the main market for DC transfer will be in highly populated areas with limited space or in sub-sea applications. With an increasing need for DC transfer in the same area a multi-terminal solution will be the better choice. A MTDC grid will limiting the number of converters and cables, reducing the cost of construction as well as operation. An increased security of supply is also achieved through alternative supply paths compared to a link construction.

A good example of such an area, suitable for a MTDC grid, is the North Sea with an increasing amount of offshore wind farms and interconnectors between the surrounding countries.

4.2 Operational Aspects

When considering the operational aspects of a MTDC grid it is important to identify the requirements and limitations of the grid. The desire is that the grid can assure a power transfer with low losses. To protect converters and cables high voltages and currents need to be limited. A low voltage is also undesirable as it would limit the transfer capability, and ability to uphold the AC voltage. The grid has to offer a secure and reliable power supply, satisfying the N-1 criteria and offering a high degree of selectivity in disconnection of faults.

The main control parameter in an MTDC grid is the DC voltage. As stated in eq. (4.1) for two arbitrary terminals connected in a MTDC grid, the active power transfer is directly linked to the voltage difference of the two terminals. Since the VSC can offer DC voltage control it means that balanced operation can be achieved with a proper voltage control scheme, further discussed in sec. 4.3.

$$P_{12} = U_1 \frac{U_1 - U_2}{R_{12}} \tag{4.1}$$

The power electronics in converters put a strict limit on high voltages, which can be a demanding task in MTDC operation. The transfer cables has a low resistance and energy storage capability giving a rapidly increasing voltage deviation during power imbalances. To keep within the limitations a fast response of the regulation is needed. The dynamic response of a MTDC system to load changes and AC as well as DC faults has been addressed in several research papers, [22], [23] and [24] to name a few. All concluding that by utilizing the fast regulation of VSC a stable operation can be achieved.

A MTDC grid can connect two completely separated AC grids with different system operators, as for instance the Norwegian and English grid in the proposed grid structure. This will make operation planning and instant power balancing more difficult. Therefore, a simple and predictable power exchange between the two grids is desirable. The planning and balancing of the wind farm production can then be done by one operator only including a certain power exchange to the connected grid.

4.2.1 Fault Clearing and Selectivity in MTDC grids

When expanding to MTDC grid another issue regarding selectivity arises. In a HVDC-link, faults in the DC cable or converters are cleared by use of circuit breakers (CBs) on the AC side to disconnect the whole link. In a MTDC grid it is desirable to keep a high selectivity by only disconnecting the faulty part. This would leave the rest of the grid operational, resulting in an increased security of supply.

In research papers there are basically two different methods presented for clearing DC faults, namely with or without DC-CBs. Without CBs imply that the AC-CBs in combination with blocking of the VSCs are used to extinguish the fault. Fast mechanical DC switches isolate the faulted line before the AC-CBs and VSCs are reconnected. In [25] this method is analyzed in combination with the handshaking method to detect and locate the fault. As stated, this method demands only small investments in mechanical DC switches, but results in a fault clearing time of about 0,5s.

To limit the fault clearing time investments in a more expensive grid design using DC-CBs has to be done. With such a grid structure the DC-CBs are used to extinguish the fault, and ideally only the CBs closes to the fault shall operate. This will result in a high selectivity and a low fault clearing time dependent upon type of CB and operation principal used. There is however no clear choice for DC-CB design especially for high voltage applications. Different CBs in combination with detection and isolation schemes are studied as compensation between fast clearing times, degree of selectivity and costs [26], [27] and [28]. It is stated that further development in this area is needed in order to assure a cost effective and reliable MTDC grid that can offer a high degree of selectivity and short fault clearing times.

4.3 MTDC Control Methods

As mentioned above the operation of a MTDC grid has to keep voltages and currents within the limitation of converters and cables. Current limitations is handled by regulation on each converter as presented in sec. 3.2.1. Operation within the voltage limitations is accomplished by utilization of DC voltage control, sec. 3.3.4.

As stated in Chapter 3 the need for regulation in AC grids differ. Therefore, not all converters connected are suitable for DC voltage control. At the same time the MTDC grid has to satisfy the N-1 criteria, which demands that the grid shall remain operative even with disconnection of a whole terminal. To satisfy these demands and limit the propagation of disturbances between the connected AC grids a number of DC voltage control methods has been presented in literature. In the following sections the basic control features will be presented and related to the proposed grid structure shown in fig. 4.2 for clarity.

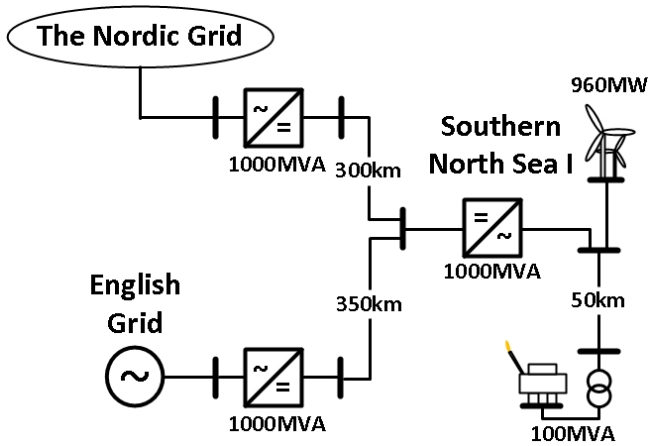

Figure 4.2: Schematic drawing of the three-terminal DC grid.

4.3.1 Voltage Margin Control

The simplest DC voltage control feature is to implement only one terminal with DC voltage control. The converter will operate as a swing bus for the MTDC grid balancing the power allowing the rest to operate with constant power control or as a swing bus for the AC grid. This demand the designated converter to be connected to a stiff grid, that can contribute with the balancing power even during disturbances.

In fig. 4.2 the terminals in Norway and England are suitable for this control. As previously stated it is desirable to have a controllable trade with England, so in the presented case Norway is chosen as the DC swing bus. Constant

power control is chosen for the terminal in England to keep a controllable power exchange. The offshore converter, Southern North Sea I, is operating as a swing bus for the offshore AC grid. This is equivalent to constant power control with a continuously changing reference.

The main operational feature is presented in fig. 4.3. There are two separate states of operation shown in the figure. One state where there is little offshore wind farm production, marked with a red circle. The other is a state where the power production is high, yellow circle. For an easier explanation voltage drop between the terminals and losses in transmission is disregarded. The terminal

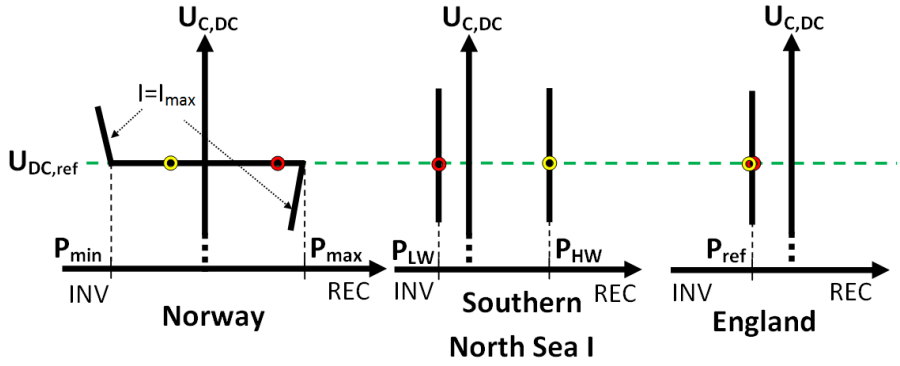

Figure 4.3: Power vs. DC voltage for each terminal with Norway operating as a DC swing bus. Two operational states high wind production (yellow) low wind production (red)

in Norway delivers the power needed to keep the voltage at its terminal equal to $U_{DC,ref}$. As the wind increases the offshore converter goes from inverter to rectifier mode. This is compensated by the converter in Norway and a new operating state is achieved.

This control feature allows for a simple and predictable exchange with England, and the offshore grid operational planning is completely connected to the Norwegian grid. However, the control feature has no means for DC voltage control when the Norwegian terminal is brought to its limits or disconnected due to a fault. By use of voltage margin control this problem can be solved.

The voltage margin control [29] imply that every terminal suitable to operate as a DC voltage swing bus is applied with a voltage reference. Each reference

has a marginal deviation according to the others so that only one terminal is designated for DC voltage control at any instance. When the terminal is brought to its limits or disconnected this would lead to a increasing or decreasing DC voltage. The terminal with the smallest margin will take over as the DC swing bus allowing for a continuous operation.

In the proposed grid structure this would mean that the English terminal is applied with an upper and lower voltage reference with a certain margin compared to the voltage reference at the Norwegian terminal. This is shown in fig. 4.4 for two operational states where there is a high power transfer to England bringing the Norwegian terminal to its limit as wind power production goes from high to low. As shown in the figure the Norwegian terminal is brought to its upper

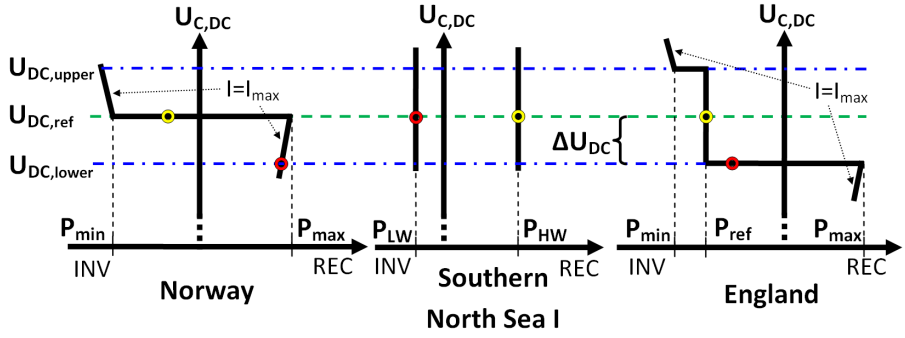

Figure 4.4: Power vs. DC voltage for each terminal with voltage margin applied. Two operational states high wind production (yellow) low wind production (red)

limit as the demand by the English and Offshore terminal is to high. A deficit of power results in a declining voltage. The voltage is reduced with ΔU_{DC} reaching the preset lower limit of the English terminal. The terminal goes from active power to DC voltage control giving a new operational state with lowered power demand.

The voltage margin method allows for a independent operation of each terminal based on preset values for voltage margins, no communication between the terminals is needed. It gives a reliable operation with only marginal voltage deviations. Large load variations and even disconnection of a whole terminal is possible. The major drawback is however that only one terminal acts as a balancing unit at any given time. This might be a good solution for small

MTDC grids with few terminals, but in large grids the deviations will become a demanding task for one terminal. This will put a sincere stress on the AC grid connected, and lead to many transitions from one swing bus to another. In [22] it is stated that the abrupt transition from one swing bus to another will imply a unnecessary stress on the system and can cause stability problems.

4.3.2 Voltage Droop Control

To tackle the drawbacks of the voltage margin control a way to delegate the power balancing on several terminals is needed. In an AC-grid this is accomplished by use of frequency-droop power-characteristic for each generating unit [30]. In [31] an analog to the frequency droop is suggested for MTDC grids with LCC converters by utilizing a voltage droop control. The voltage droop control has been further applied in research of MTDC grid with VSC in [32] and [33].

The principal difference between voltage margin and droop control is shown in fig. 4.5. As shown in the figure the terminal does not keep a constant voltage

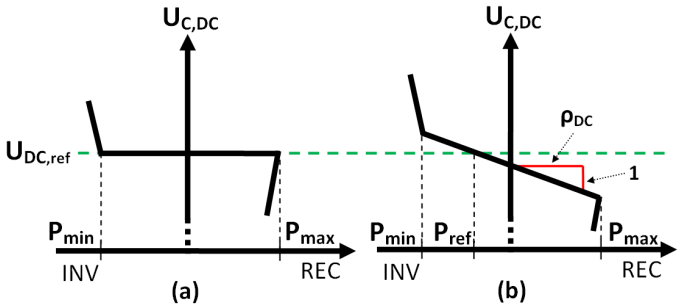

Figure 4.5: Power vs. DC voltage for the two control methods voltage margin (a), and voltage droop (b)

with varying power. Instead a certain droop in voltage according to power is applied, described by eq. (4.2).

$$U_{C,DC} - U_{DC,ref} = -\rho_{DC}\,(P - P_{ref}) \tag{4.2}$$

By assigning several terminals with this control feature a change power will be divided between the terminals according to their droop. For the proposed grid structure this could be applied to the terminals in England and Norway allowing the wind production deviations to be divided between the two terminals.

The voltage droop control would lead to reduced stress on the Norwegian grid, and no DC voltage steps would be experienced as one of the terminals reaches its limit. However, the power delivered to England would no longer be controlled.

Merged DC Voltage Control

In [33] a third control feature was presented that combines voltage margin with the voltage droop. The idea is to leave a deadband in voltage where the terminal is controlled at constant current, or as presented in fig. 4.6; power. If the DC voltage reaches one of the preset limits the terminal switches to voltage droop control in order to prohibit the voltage to reach undesirable levels.

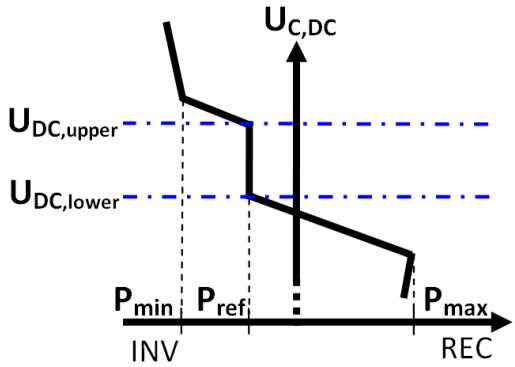

Figure 4.6: Power vs. DC voltage for a terminal with a merged DC voltage control

This control feature can be applied to the terminal in England with the Norwegian terminal operating with either droop or marginal control. Figure. 4.7 presents the two operational states shown in fig. 4.4 with the Norwegian terminal operating with droop control and the English terminal with merged control. The English terminal will operate with a constant power for almost all states

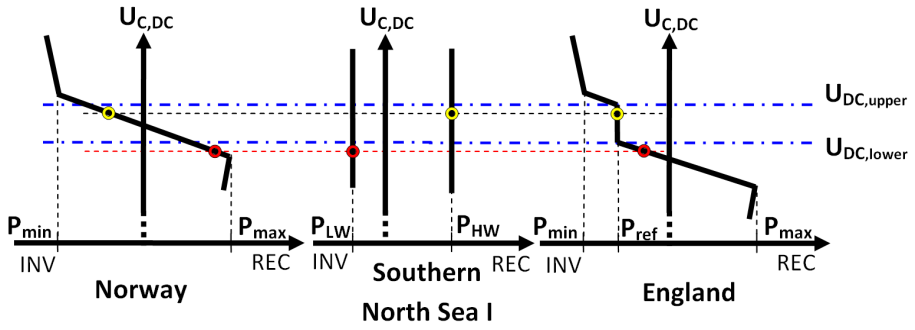

Figure 4.7: Power vs. DC voltage for a terminal with voltage droop control in Norway and merged DC voltage control in England

giving a predictable power exchange. As the Norwegian terminal has droop control the voltage will change according to the balancing power given. When the voltage reaches the preset limits on the English terminal it switches to droop control assisting the Norwegian terminal to balance power. As can be seen this prohibits the Norwegian terminal from reaching its power limit in the given case. This control feature allows for a predictable power exchange to England. There are no abrupt changes in DC voltage and unnecessary stress on the Norwegian grid is prohibited.

Chapter 5

System Models and Simulation Software

This chapter will shortly present the argumentation for the simulation software used, its general structure and limitations in modeling. Further will the different models implemented be explained. Dimensioning parameters for the components of the grid will be given.

5.1 The Simulation Software SIMPOW

One of the major tasks for this thesis was establishing simulation models of the multi-terminal DC grid and the offshore converter stations. Analysis of the MTDC grid and its influence on the connected AC grids where of interest. The simulation tool chosen for the task where SIMPOW as it is found to be a suitable program to perform analysis on such large systems. The decision where reinforced since the work were to be performed in cooperation with Solvina, that have experience with the use of SIMPOW.

SIMPOW is built to perform power flow-, fault current- and electromechanical transient stability analysis of electrical systems [34]. It consists of several modules which perform the different analysis. The module DYNPOW is used for dynamic simulations and is split into two parts. One part is MASTA performing

calculations with instantaneous values. In this thesis however the TRANSTA part is utilized.

TRANSTA uses phasor representation of voltages and currents in the AC system and mean values in the DC system. Reactances are used for representation of capacitances and inductances in the AC system, giving complex algebraic equations for system calculations. This simplifies the implementation of transformers, cables and electrical machines, but exclude the electromagnetic phenomena with oscillations between gird capacitances and inductances. Only the first harmonic of converters are represented, excluding discrete switch representation. As a consequence a complete model of the entire system is possible, although at the cost of accuracy for short time frames. However, in the DC system capacitances and inductances are included, giving differential equations for state variables. This allows for a more accurate calculation of the DC system dynamics dominated by the charging of cable capacitances.

The module called OPTPOW is where the system topology is specified. It performs steady-state calculations for power flow analysis. This offers a way to identify critical states of the system, and provide an initial condition for the dynamic simulations in DYNPOW.

5.2 Three Terminal DC grid

As previously stated the complete grid structure shown in fig. 1.1(b) has been limited to the three-terminal structure, re-given in fig. 5.1 for clarity. The model can be divided into four parts, the Nordic grid, offshore AC grid, English grid, the MTDC grid with the VSCs and regulation connecting all the parts together. The implementation of each part and their interconnection has been performed in order to bring out the system characteristics relevant for the analysis. Limitations have been done to reduce the complete model size and complexity.

This thesis has been accomplished in cooperation with Statnett, and as such, assumed that Statnett shall operate the grid allowing the Nordic grid connection to serve as a swingbus for the MTDC grid. Such a connection will demand a strong grid which can handle the perturbations inflicted during operation and fault scenarios. The Nordic grid has therefore been modeled with a 35-node equivalent, presented in sec. 5.5.

The Offshore AC grid structure where built by Solvina. They have focused

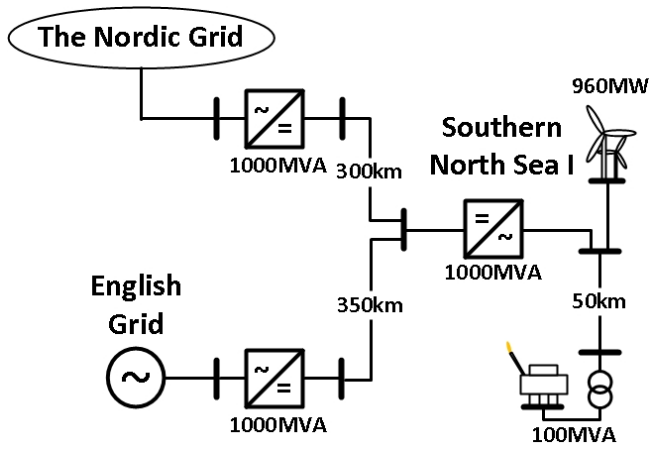

Figure 5.1: Schematic drawing of the three-terminal DC grid.

on dimensioning criteria in fault situations for the complete offshore AC grid supplied by two VSCs [6]. The offshore AC grid operation was not in the scope of this thesis, and hence, the model built by Solvina was reduced to an equivalent with one wind farm and oil platform. This is done to keep a similarity in the two parallel works, giving an easier and more reliable comparison. See section 5.4 for the implementation of the offshore AC grid.

The English grid connection was analyzed in concern of how the power exchange were affected by the MTDC-grid operation, but not the influence of the English grid itself. The grid was therefore represented by a single AC node, with a stiff voltage at 300kV, able to supply or consume any active and reactive power desired. The converter station where implemented with active power control allowing a controlled power exchange. Reactive power control where set to a minimum.

5.3 Converter Station and DC grid

Each terminal, in the MTDC-grid, were implemented with the same converter *station* model, fig. 5.2, but with different control features applied as to fit the behavior and demand of the AC grid they are connected to.

The labeling in fig. 5.2 is given as for the converter station in Norway, and will hence be _SNI and _EN for Southern North Sea I and English converter stations, respectively. There are basically three main components which make up the station; converter, transformer and filter. The line between MCON_NO and BUS1_NO is a line without resistance or reactance added for measuring the active and reactive power delivered to the AC grid.

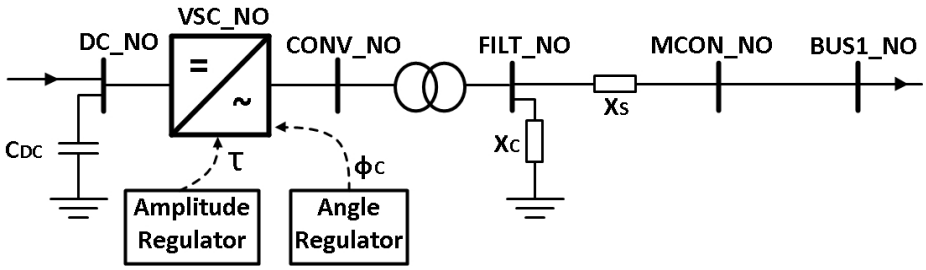

Figure 5.2: Schematic drawing of Converter Station model.

All three converters have a rating of 1000MVA and a nominal AC voltage of 400kV and DC voltage of 640kV. The DC voltage level where chosen as a single line equivalent of a bi-pole construction with a voltage of $\pm$ 320kV. The converters are specified with resistances $R = 0.01$ and $RP = 100$ for loss calculations according to eq. (3.3). The values result in 1% no-load losses and an additional 1% load dependent loss under rated conditions.

Figure 5.2 show that the transformer is directly connected to the VSC. In practice the AC-filter is placed at the terminals of the converter, before the transformer, in order to protect it from the high frequency components of the converter output. However, as specified in [35] the predefined model demand the filter to have the same nominal voltage as the station terminal. The filter and transformer have therefore switched places in the model and the filter has been scaled accordingly, see Appendix 10 for calculations. As the model only considers the first harmonic components this has no influence on the simulation result.

The transformers are implemented as regular two winding transformers, specified by their short circuit resistance and reactance. The values are given in pu of the transformer nominal power and voltage. The turn ratio is specified by the ratio of the given primary and secondary voltages. The AC-filters are rep-

resented by a shunt and series reactance. The DC cables are modeled as series resistances and a DC-shunt capacitance is added to each connected terminal. The shunt at each end of a cable represents half the cable capacitance as well as the converter DC filter capacitance. The parameters for all components are presented in Appendix 10.

5.3.1 Converter Regulation and Tuning

As stated in Chapter 3 each converter can contribute with a number of different control features by implementing regulation for τ and ϕ_C. The dynamic behavior of the converters will therefore be dependent upon the tuning of these regulators. The regulators added to each terminal is presented in the tab. 5.1. All regulators applied are PI-regulators with a low-pass filter on the measured

Converter Station:	Regulators:
Norway	Phase angle *and* DC-voltage *and* AC-voltage *or* Reactive Power
Southern North Sea I	Phase angle *and* AC-voltage
England	Phase angle *and* Active power *and* Reactive Power

Table 5.1: Regulators implemented for each converter station

value. The parameters to be tuned where the gain K_P, the integration time constant T_i and the time constant T_F of the low-pass filter. For the phase angle regulator $T_F = 0.25ms$ to represent the time delay of a VSC with an equivalent switching frequency of 2000Hz. All the other regulators where implemented with $T_F = 0.01$s assuming that fast measurements in half a system period is possible.

A model of the converter station, fig 5.2, connected to a stiff node on both the AC and DC side where used to study the effect of K_P and T_i. The connection consisted of a cable equivalent on the DC side, represented by a series resistance and a shunt capacitance with the same values as for the cable between the Nordic

grid and the offshore converter station. On the AC side the connection was made with π-equivalent representing a line connection. The parameterization of the model is described in the simulation files given in Appendix 11. A trail and error procedure where performed, analyzing the response for the converter when applying a step in reference values. The response to different K_P values is illustrated in fig 5.3 for a converter implemented with DC-voltage control. In the figure a step is applied in DC-voltage reference bringing the desired voltage value from 638kV to 642kV on the station terminal. The integral time constant where kept at 20μs to isolate the effect of K_P. The figure show that an increasing K_P

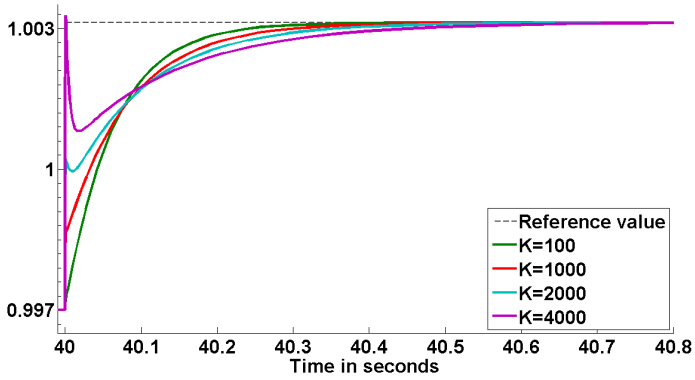

Figure 5.3: DC-regulator step response according to different K_P values, where $T_i = 20\mu s$.

result in less initial deviation from the reference. However, this reduction will lessen the deviation to be integrated resulting in longer time before stationary conditions are reached. For the higher K_P values a overshoot can be observed. This is because the fast initial response is influenced by the low-pass filter on the measured feedback.

In figure 5.4 a similar procedure were performed except here $K_P = 1000$ and T_i where altered. The integral time constant basically scales the effect of integration. For a high value the integral effect is low, resulting in a slow response. As T_i is reduced the response become quicker, and even contributes to overshoot and a oscillatory response.

When choosing the parametrization, speed and accuracy has to be leveled against inflicted perturbations on the system. A fast DC-voltage regulation

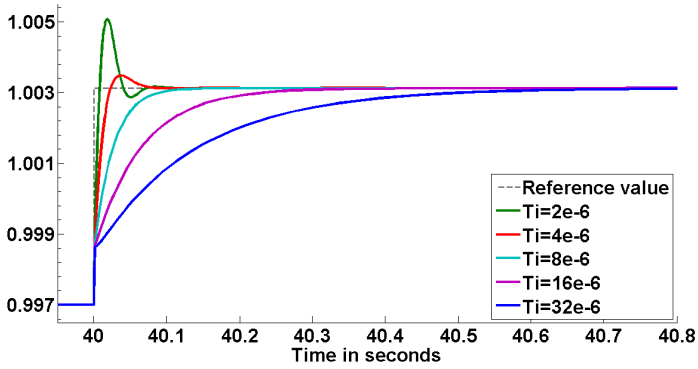

Figure 5.4: DC-regulator step response according to different T_i values, where $K_P = 1000$.

will almost directly inflict perturbations on the DC side onto the AC side. For AC-voltage regulation a fast response would lead to demanding changes in reactive power supplied by the converter. Implementing a slower response will result in a weaker link of the two grids and less stress on the supply. However, this can give large deviations from reference values for a considerate amount of time. The phase angle regulator is operating as a inner regulation loop, creating a set point for outer regulation being either DC-voltage or active power control. The regulator were therefore chosen to have a fast initial response as not to prohibit the outer control operation. The feedback for the phase regulator is also directly connected to the output minimizing the influence of the grid behavior and allowing a fast response. Parameterization for the phase angle regulators in all three converter station where chosen equal and is presented in tab. 5.2.

The active and reactive power regulator for the English terminal as well as the reactive power regulator for the Norwegian terminal were chosen to be relatively slow, reaching a stationary solution for the step response in about a second. The AC regulation were on the other hand tuned to be as fast as possible without creating oscillations. DC-voltage regulation demands a quick handling to prevent high DC voltage. Stated in Chapter 3 deviations in DC power flow is equivalent with charging and discharging the DC capacitors. As these capacitors have a small storage capability, compared to the transferred power, large voltage oscillations will occur if not regulated quickly. Equation (5.1), [35], calculates the time for the DC capacitor to fully discharge when a deviation in power,

ΔP, occurs. With a total capacitance of 119.8μF this gives a time constant of 24.5ms for the DC system.

$$T_{DC} = \frac{1}{2}\frac{C\,U^2}{\Delta P} \tag{5.1}$$

Considering the equation for power flow in a DC cable (4.1) and the low resistances given in tab. 10.6 it gives a relation of $170MW/kV$ for the cable between Norway and the Southern North Sea I, when operating at nominal voltage. With such a steep relation between power exchange and voltage deviation combined with the low DC cable time constant the DC regulation where tuned as fast as possible, giving a small overshoot without resulting in oscillations. As presented in tab. 5.2 a slower DC-regulation response where also chosen to study the effect of regulation speed. All step responses are given in Appendix 10.

Station	Regulator	T_F [ms]	K_P [pu/pu]	T_i [ms]
Norway	Phase angle	0.25	50	1.0
	Fast DC-voltage	10	3000	0.003
	Slow DC-voltage	10	100	0.3
	Reactive Power	10	0.2	100
	AC-voltage	10	0.5	20
Southern North Sea I	Phase angle	0.25	50	1.0
	AC-voltage	10	0.5	20
England	Phase angle	0.25	50	1.0
	Active power	10	10	2.0
	Reactive Power	10	0.2	100

Table 5.2: Regulator parameters for the Norwegian converter station.

As stated in sec. 3.2.1 all converters were implemented with a current limit regulator. The converter station model was applied with a three-phase fault for 70ms at the AC terminal BUS1_NO, in order to study the regulator response. The absolute value of the converter current where observed, and the regulator parameters where tuned in order to keep the current at rated value. It was noticed that the time constant for the low-pass filter had a large influence on the response, so it were reduced to 1ms in order for the regulator to have an effect. The low-pass filter still causes the large overshoot which is shown in figure 5.5. The gain and integral time constant chosen are given in table 5.3. The same value were implemented for all three converters and for both the amplitude limiter and phase angle limiter.

T_F [ms]	K_P [pu/pu]	T_i [ms]
1	5	5.6

Table 5.3: Current limit regulator parameters implemented for all three converters.

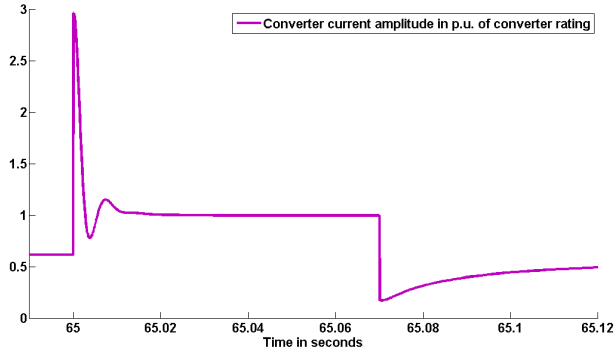

Figure 5.5: The absolute value of the converter current given in p.u. of 1443A.

5.4 Offshore Grid

The offshore AC grid in the proposed structure, fig. 1.1(b), where composed of two oil platforms and two wind farms which where supplied by two HVDC-VSC terminals. Since the thesis analysis focused on the MTDC-grid operation a simplified grid with one wind farm and oil platform were implemented. This simplification is further supported as the cable connection to the oil platforms were not rated for power transfer between the two HVDC-VSCs or wind farms. A schematic drawing of the offshore AC grid is shown in fig. 5.6. Notice how the complete converter station is represented as one component, with only the connection terminals DC_SNI and BUS1_SNI given.

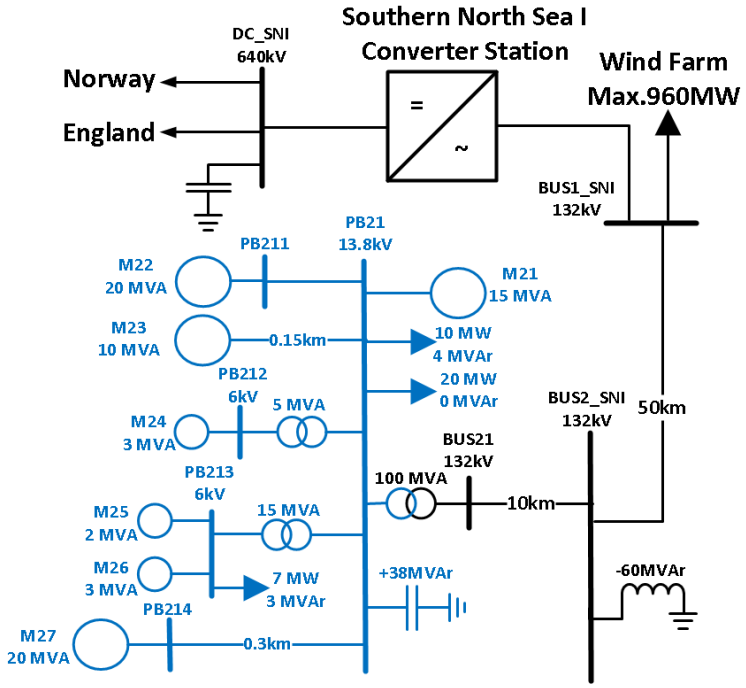

Figure 5.6: Schematic drawing of the offshore AC grid. The oil platform is presented in blue.

5.4.1 Oil Platform

The oil platform model is based on a model used in [36], but has been modified by Solvina [6]. The platform has an approximate rating of 100MVA divided between seven direct driven asynchronous machines and three pure active- and reactive power loads. The main voltage level is 13.8kV while the two nodes PB212 and PB213 are operating at 6kV. All three transformers are regular two winding transformers. A tap-changer has been added on the transformer between PB21 and PB213 to keep nominal voltage at PB213. To compensate for the reactive power demand of the asynchronous machines a shunt capacitor has been connected to the main busbar PB21 supplying 38MVAr at nominal voltage. The cables both within the platform and for the 132kV supply transmission are modeled as π-equivalents. Due to the reactive power production of the 50km long supply cable a shunt reactor, consuming 60MVAr at nominal voltage, where added to the connection node BUS2_SNI. For further details on model parameters see Appendix 10.1

5.4.2 Wind Farm

Originally the idea were to use a wind farm model built by Solvina. The model consist of three aggregated turbines with a rating of 20, 140 and 800MW, giving a total wind farm capacity of 960MW. It was assumed that the wind farm consist of full-converter wind turbines, allowing complete control over reactive power production within converter rating. Therefore the wind farm where modeled as a controllable current source, adjusting the injected current according to desired active and reactive power production. Further details on the model are described in [6].

Simulation difficulties were experienced when initializing the wind farm model in cooperation with the HVDC-VSC models. The wind farm had to be modeled as a pure active power supply on the converter station connection node, BUS1_SNI. The rating of the power supply was 960MW, and production values were specified according to time through a user specified input table. No reactive power production were added, assuming that the reactive power control of the full-converter wind turbines where utilized to operate with a unity power factor.

5.5 The Nordic Grid

A key goal for the thesis were to see how a stable MTDC grid operation could be assured, and again what affect this would have on the connected AC grids. Especially of interest is the behavior in the Nordic Grid as the connecting terminal were to operate as a swingbus for the DC system. In order to study this, an equivalent model of the Nordic Grid were integrated.

The Nordic Grid model has been built by SINTEF Energy Research [37] in the simulation tool PSS/E. The model developed in steps from a 15-node equivalent of the Norwegian and Swedish grid based on work done in [38], to a 23-node equivalent [39] including representation of Germany, Denmark and Finland. As SIMPOW was utilized, a 22-node equivalent converted from PSS/E to SIMPOW by Guillaume Verez [40] were chosen. The model is identical to the one in [39] except no representation of the asynchronous grid in Germany and Jutland. The DC-cable connections to Jutland and between Sweden and Finland are however represented by loads at the connection nodes.

A illustrative drawing of the model is shown in fig. 5.7. The model consists of 35 nodes in total, distributed over three different voltage levels, 420kV (dark blue), 300kV (pink) and 135kV (orange). The 22 numbered nodes in the figure were chosen connection points, in the real Nordic grid, to bring out characteristic features of large production and consumption areas as well as bottlenecks in the main transmission grid [41]. Among these nodes 20 generators and 19 loads are connected, representing the production and consumption of underlying regional and distribution grids. Additional loads are added to the nodes 3000, 7000, 3360 and 5603 representing the DC-cable connection between Sweden and Finland and the exchange with Jutland. All the loads are specified with a certain initial active and reactive power, and a voltage relation given in eq. (5.2) and (5.3)

$$P = P_0 \left(\frac{U}{U_0} \right) \tag{5.2}$$

$$Q = Q_0 \left(\frac{U}{U_0} \right)^2 \tag{5.3}$$

Transmission lines in the grid are represented as π-equivalents described by the resistance (R), inductance (X) and susceptance (B) as shown in fig. 5.8. The conversion between PSS/E and SIMPOW demanded some additional shunt impedances to be added as a part of the line implementation [40]. These shunts

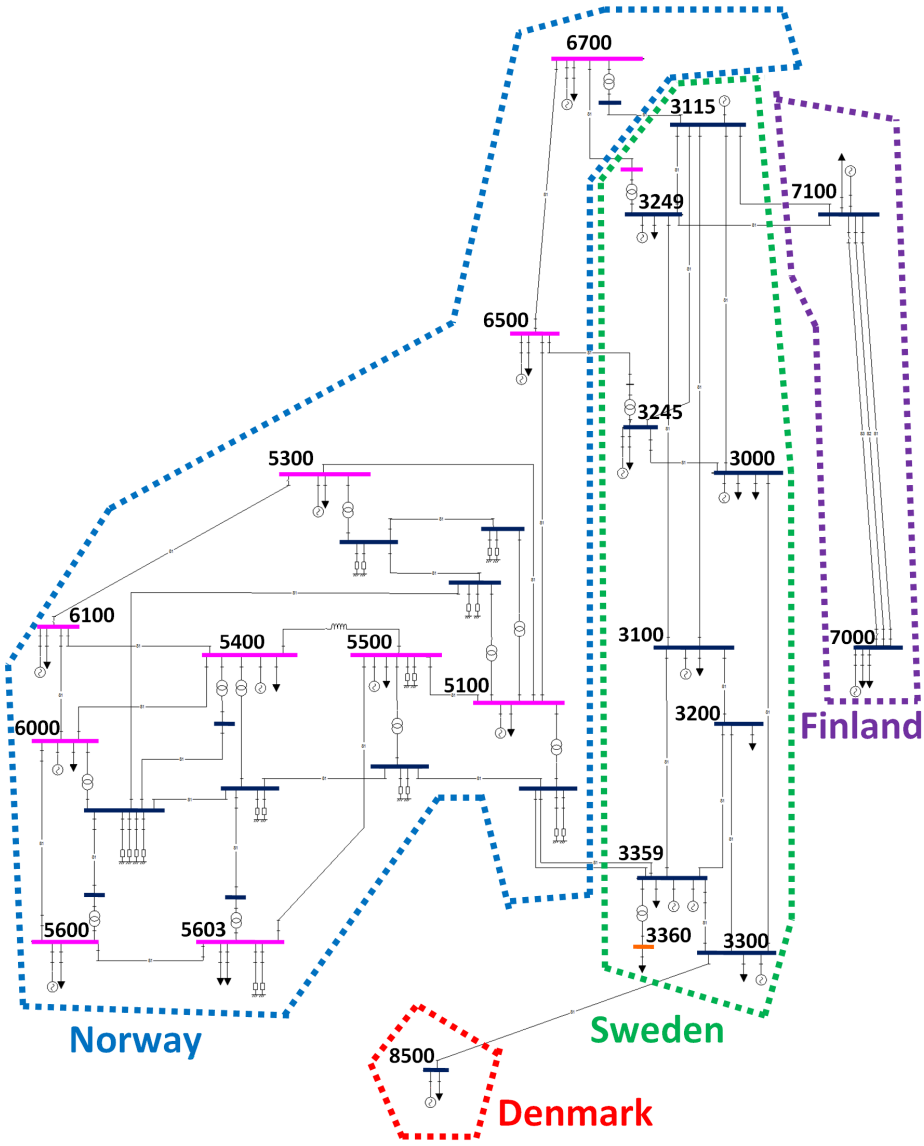

Figure 5.7: Schematic drawing of the Nordic grid model [40]. The numbered nodes are connection points representing areas of production and consumption. The nodes have different colors according to voltage; 420kV (dark blue), 300kV (pink) and 135kV (orange).

can be seen at the 420kV nodes in Norway. The individual values for each line and shunt is presented in Appendix 10.2. Stated in [41] the lines have been scaled in order to imitate the power flow simulations performed in [42]. Therefore, the parameterization of the different lines are not representative for a single transmission line.

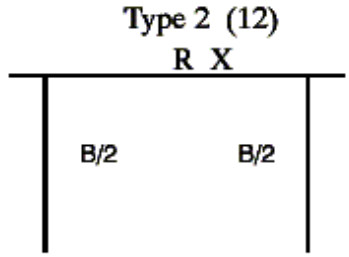

Figure 5.8: The line model used in the Nordic grid [34]

The power production in the Nordic grid consist primarily of hydro power in Norway and northern Sweden, and nuclear power plants in southern Sweden and Finland. The power production units in the equivalent model is therefore implemented with either a hydro power model or a thermal power model. Both models are made up of a turbine, governor, generator and exciter. A few units is also equipped with a power stabilizer. Table 5.4 shows a list of the different production units, their type and rating. Also shown is which exciter and stabilizer model is implemented.

As the operation and modeling of the power production units where not in the scope of this thesis, no theory or detailed explanation will be presented. However, a short presentation and block diagrams of the models implemented is given, to give a better understanding for the level of detail. Parameterization of the components is given in Appendix 10.2. For interested readers, theory and explanation of model parameters are described in [43].

5.5.1 Generator, Turbine and Governor Models

The generators are implemented with standard synchronous generator models in SIMPOW [44]. The hydro-power generator is modeled with type 2, includ-

Node	Type	Rating [MVA]	Exciter	Stabilizer
3300	Thermal	5000	ST3	STAB2A
3000	Thermal	5579	IEEET2	STAB2A
3100	Hydro	1579	ST3	None
3115	Hydro	3758	ST3	STAB2A
3245	Hydro	822	ST3	None
3249	Hydro	5000	ST3	None
3359-1	Hydro	2811	ST3	None
3359-2	Thermal	874	ST3	STAB2A
5100	Hydro	1558	BBC1	None
5300	Hydro	2395	ST3	STAB2A
5400	Hydro	1672	BBC1	None
5500	Hydro	872	BBC1	None
5600	Hydro	2504	ST3	STAB2A*
6000	Hydro	1189	BBC1	None
6100	Hydro	2470	ST3	STAB2A*
6500	Hydro	1591	BBC1	None
6700	Hydro	2917	ST3	STAB2A
7000	Thermal	5579	IEEET2	STAB2A
7100	Hydro	1379	ST3	STAB2A
8500	Thermal	1056	ST3	STAB2A

Table 5.4: The type, rating, exciter and stabilizer of the generation models added to the Nordic grid. * are added or altered in this thesis work, see sec. 7.2

ing representation of one field and damper winding in the d-axis, and a single damper winding in the q-axis. A generator model of type 1 is used for the thermal units. Compared to type 2 this model has a representation for additional damping in the q-axis. According to [38] this is included to represent the extra damping caused by induced currents in the solid steel rotor of turbo-generators, which are common for thermal power generators. Both models include representation for saturation.

A turbine model is used to give the generator torque input, T_M. For the thermal units the standard turbine model called ST2 [45], shown in fig. 5.9(a), is implemented. It is a general model of a double-reheat tandem compound steam turbine. Each turbine stage is represented by a time constant, $T_{1\text{-}4}$, and a gain, $K_{1\text{-}4}$, which has to satisfy eq. (5.4).

$$K_1 + K_2 + K_3 + K_4 = 1.0 \tag{5.4}$$

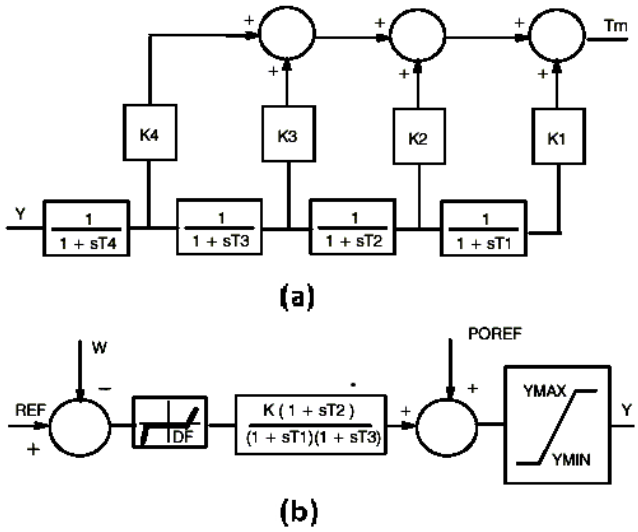

Figure 5.9: Turbine model used for thermal power units, type ST2, (a). Corresponding governor, type SG3, (b). [45]

The governor which contributes with the input value for the steam turbines, Y, is modeled with the type SG3 [45] shown in fig. 5.9(b). However, it is assumed

that the thermal power plants does not contribute with primary control, which imply that the governors can be disconnected by applying zero gain, K=0.

For the hydro-power units the turbine model DSLS/HYTUR [45], and the governor DSLS/HYGOV [45] were used. A block diagram of the two models is represented in fig. 5.10 (a) and (b), respectively.

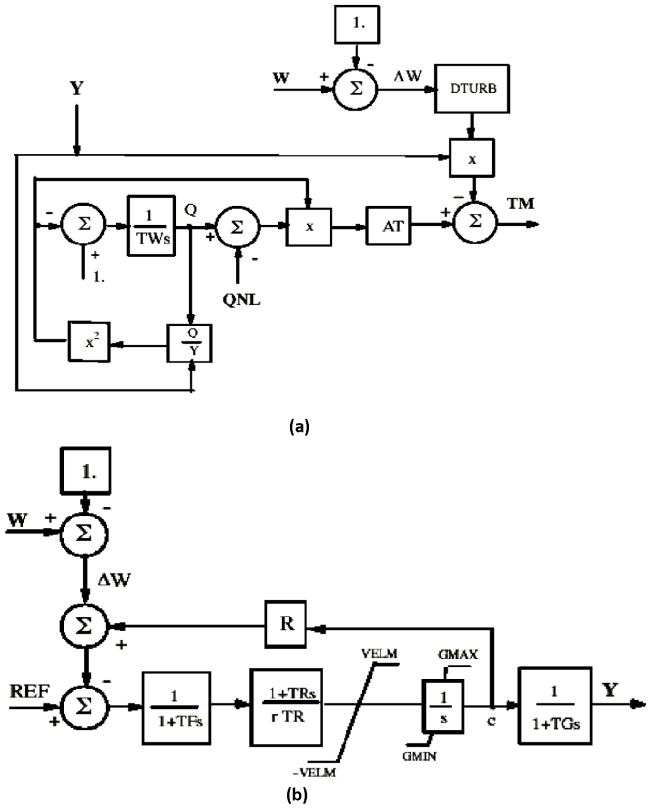

Figure 5.10: Hydro turbine model, DSLS/HYTUR, (a). Hydro governor model, DSLS/HYGOV, (b). [45]

5.5.2 Exciter and Stabilizer Models

As given in tab. 5.4 there are three different types of exciter models implemented, taken from the standard models in [46]. All three models have the aim to adjust the machine field voltage in order to keep the generator terminal voltage according to a specified reference value. However, the three models are implemented to represent different physical exciters, capabilities and dynamic responses of these. A block diagram of the three exciter models are presented in fig. 5.12.

A number of the production units are equipped with power system stabilizers (PSS), which introduced a feedback of the generator output power to the exciter, reducing system power oscillations. The PSS model utilized is the SIMPOW model STAB2A shown in fig. 5.11.

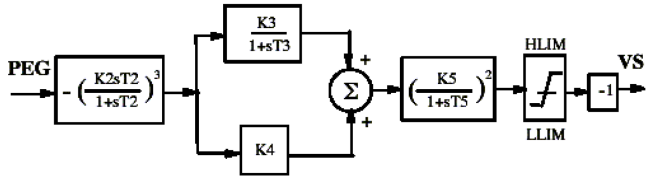

Figure 5.11: Power system stabilizer model [46]

5.5.3 Connection to the MTDC Gird

The proposed three-terminal DC grid were to be connected in Kvilldal, which is located at the south-west coast of Norway. From a geographical consideration this is equivalent to node 6000 in the Nordic grid model, and hence it was chosen for connection as shown in fig. 5.13. Illustrated in the figure are seven areas which make up the whole south part of Norway. The areas represent different regions; north-west (A61), west (A60), central (A53-55) south (A56) and east(A51). The connection area, A60, and the five areas it is directly connected to are marked with purple color, this includes A01 which is the converter station exchanging power with the MTDC grid. The MTDC grid is again divided into A02 and A03 to represent the offshore AC grid and the English grid. The different voltage levels are also separated by color, 420kV (dark blue), 300kV (pink), 400kV connection in converter station (green) and 640kV DC voltage (black).

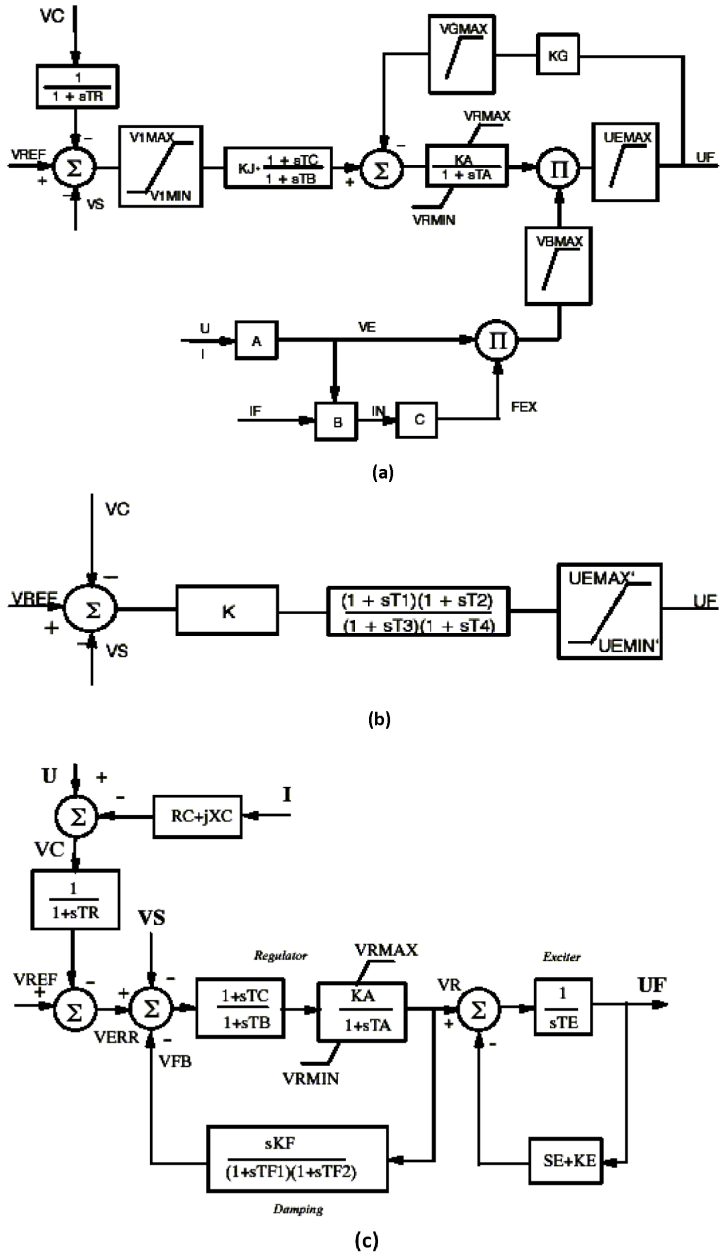

Figure 5.12: Exciter model: ST3 (a), BBC1 (b) and IEEEX2 (c) [46]

To limit the analysis and data presented further discussions will concentrate on the areas marked in purple.

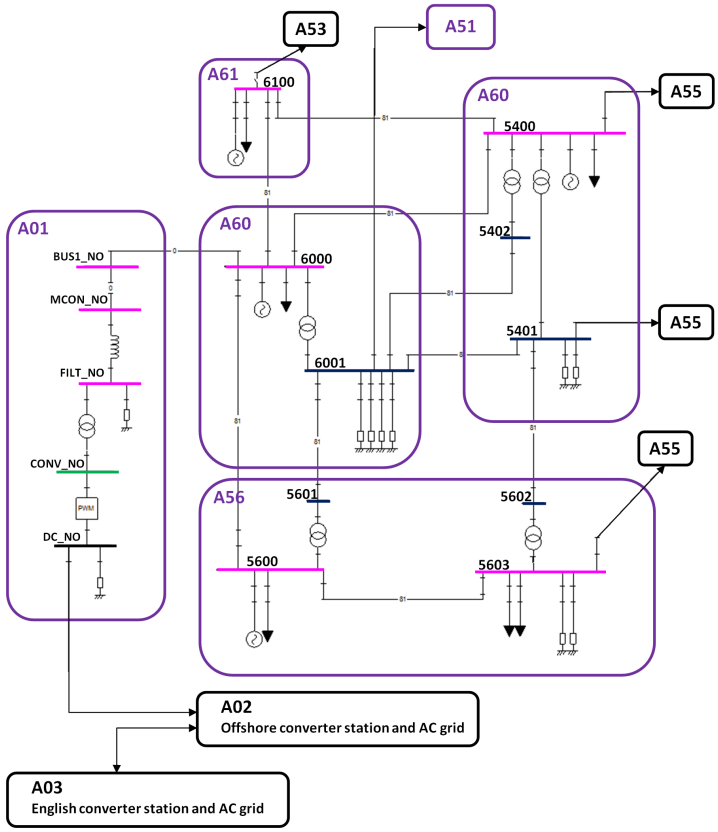

Figure 5.13: Illustration of MTDC grid connection and connecting areas in the Nordic grid

Chapter 6

Power Flow Simulations

This chapter will present the power flow simulations performed in order to identify the steady state operational limits of the MTDC-grid. Also, initial conditions chosen for the dynamic simulations performed in Chapter 7 will be presented.

6.1 Limitations for MTDC-grid Operation

Power flow simulations were performed in order to identify the limits for steady state operation of the MTDC-grid. During the simulations the oil platform loading was kept constant. The machines were operated at 75% of their rating, giving a total load of 91MW and −3MVAr at the node BUS2_SNI. Three scenarios of wind production were studied; maximum production at 960MW, no wind prodction and a marginal wind production supplying the load and losses in the offshore AC grid.

The limiting factor for power transfer is the current rating, at 1443kA, for each converter. However, the current amplitude is dependent upon both the active and reactive power supplied on the AC side of the converter. During the power flow simulations both the English and Norwegian converter station were operated with reactive power control. The control feature was implemented to keep the reactive power supply at the *station* terminals equal to zero. This

imply that the converter has to balance the reactive power of the filter and transformer, giving a reduced capability of active power exchange.

The Norwegian converter station where operated as the DC-swingbus, keeping the DC voltage at nominal value, 640kV, by adjusting the power import. Active power control where implemented on the English converter station, while the offshore converter station was operated as a AC-swingbus, adjusting the active power to balance the offshore AC-grid. It was also equipped with AC voltage control keeping nominal voltage at the station terminal BUS1_SNI.

Each wind scenario gave a certain flow in the MTDC-grid, balanced by the Norwegian converter station in order to keep nominal DC-voltage. The active power control of the English converter station was used to adjust the power exchange to both maximum *import* and *export* until either the Norwegian or English converter was operating at it's current limit, thus giving the limits of stationary operation.

Table 6.1 show which converter reaches it's limit for the different load scenarios. It emphasizes how the wind production has an effect on the power exchange. For maximum wind production the converter station which is importing power reaches it's limit first. However during marginal or zero wind production it is the converter exporting power which reach it's limits. This is because it has to supply both losses and the exchanged power.

	Max. Wind	Marginal Wind	Zero Wind
Max. Import	VSC_EN	VSC_NO	VSC_NO
Max. Export	VSC_NO	VSC_EN	VSC_EN

Table 6.1: The table show which converter is operating at it's limit for the different power flow scenarios. The export and import is viewed from the English terminal as it is the terminal adjusting the power.

To see more clearly the power exchange that is attainable the active and reactive power supplied, by each converter to it's AC-grid, is given in tab. 6.2. Studying the English terminal it is evident that a relative low export is accomplished compared to the converter rating. The opposite effect is seen at the Norwegian terminal, which is able to import and export active power higher than its rating. This is linked to the voltage at the converter terminals effecting the power capability during rated current, shown in tab. 6.5. The losses of the transmission and converters corresponding to the different power flow is given in tab. 6.3.

		Max. Wind	Marginal Wind	Zero Wind
Max. Import	VSC_NO [MW]	-147	-1019	-1015
	VSC_NO [MVAr]	-145	147	147
	VSC_SNI [MW]	-866	-0.01	94
	VSC_SNI [MVAr]	54	-180	-177
	VSC_EN [MW]	955	950	855
	VSC_EN [MVAr]	154	150	82
Max. Export	VSC_NO [MW]	1021	818	725
	VSC_NO [MVAr]	135	35	-5
	VSC_SNI [MW]	-866	-0.01	94
	VSC_SNI [MVAr]	54	-180	-177
	VSC_EN [MW]	-215	-876	-876
	VSC_EN [MVAr]	-133	180	181

Table 6.2: Active and reactive power supplied by each converter to it's AC grid, during maximum import to and export from the English terminal. The values are presented for three different offshore wind farm productions; maximum power production, zero production and a marginal production supplying the load and losses of the offshore AC grid.

		Max. Wind	Marginal Wind	Zero Wind
Max. Import	$P_{loss,tot}$ [MW]	47.111	49.611	47.672
	$\mathrm{DC}_{line,losses}$ [MW]	10.802	20.036	17.897
	Total losses [%]	5.717	6.830	6.461
Max. Export	$P_{loss,tot}$ [MW]	48.506	44.599	43.237
	$\mathrm{DC}_{line,losses}$ [MW]	10.617	14.302	12.929
	Total losses [%]	5.471	6.717	6.412

Table 6.3: The table show the total transmission and converter losses for each power flow scenario. The losses are presented in MW as well as in percentage of the power supplied to the MTDC-grid.

Each converter is, as stated in sec. 5.3, implemented with a certain loss dependent upon the voltage and current at the terminal. Given in tab. 6.4 is the maximum and minimum values for these losses, as well as the measured losses of the HVDC transmission. The minimum values correspond to a no-load situation with marginal wind and zero exchange with England.

	Maximum Value [MW]	Minimum Value [MW]
Converter P_{loss}	20.83	9.77
Transmission loss	20.0	0.0034

Table 6.4: The table show the maximum and minimum losses for a single converter and for the HVDC transmission.

To further identify the frame of operation the maximum and minimum values for DC- and converter voltages are presented in tab. 6.5. Noticeable is the low voltage for the English AC-grid, caused by the combination of the transmission line connecting the converter station to the node BUS2_EN and the control feature keeping zero reactive power supplied by the converter station.

Node	Maximum Value [pu]	Minimum Value [pu]
CONV_NO	1.03231	0.987417
CONV_SNI	1.01051	0.971178
CONV_EN	0.98242	0.895145
BUS1_NO	1.00825	0.999576
BUS1_SNI	1.0	1.0
BUS1_EN	0.99592	0.860528
DC_NO	1.0	1.0
DC_SNI	1.00976	0.990647
DC_EN	1.01703	0.979842

Table 6.5: The table show the maximum and minimum voltages observed during the power flow calculations.

6.2 The Initial Power Flow

A power flow simulation was performed to give an initial condition for the dynamic simulations performed in the TRANSTA part of SIMPOW. For the MTDC-grid a scenario was chosen, where the wind farm was producing 700MW and the English terminal was operated with an import of 200MW. The reactive power control of the English and Norwegian converter station was operated in order to minimize the exchange of reactive power. This resulted in the power flow, and voltages given in fig. 6.1. As fig. 6.1 show, the scenario chosen results

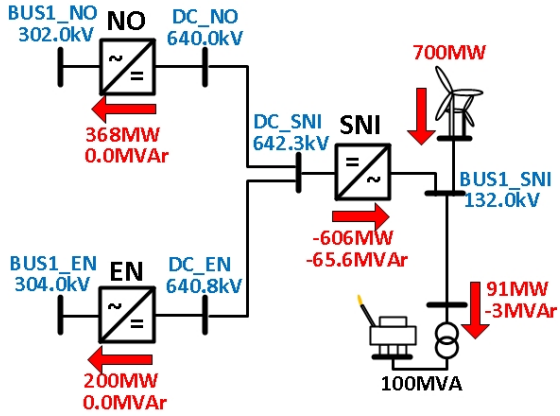

Figure 6.1: The initial power flow for the MTDC-grid used for dynamic simulations.

in an import to the Nordic grid of 368MW.

Originally the Nordic grid had an power flow, adjusted in [41], to fit the power flow in the Nordic grid at an arbitrarily chosen day. To give a perspective of the model size the aggregated production and load for each country is given in tab. 6.6.

The load and production for the selected areas and their power exchange is shown in fig. 6.2. This power flow will be used as an initial condition in the *Base Case* of the dynamic simulations, further discussed in sec. 7.2.

In the power flow calculations the production and load are given control parameters, and a single generator, at node 3300 in the Nordic grid, is chosen as a swingbus balancing the active and reactive power. Therefore, when introducing

	Production		Load	
Country	P [MW]	Q [MVAr]	P [MW]	Q [MVAr]
Norway	16306	3880	17147	3335
Sweden	24302	9950	21160	4130
Finland	6610	1671	8100	1650
Danmark	1000	910	1000	1000

Table 6.6: A table showing initial active and reactive power production and load for each country in the Nordic grid.

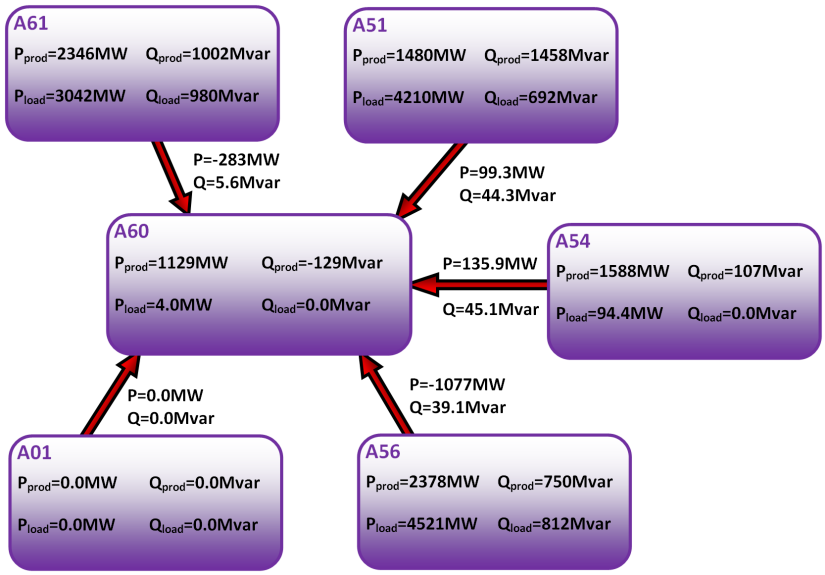

Figure 6.2: The power flow, taken from [41], for the selected areas in the Nordic grid.

the import of 368MW from the MTDC-grid this will alter the initial condition of the Nordic grid, transporting the access power to node 3300. To give a more realistic power flow it was assumed that the import would lead to reduced production in the generators closest to the connection point. The import from the MTDC-grid were thus divided among the generators in the selected areas, as shown in tab. 6.7, giving a new initial power flow shown in fig. 6.3.

Node	Reduction [MW]	New Production [MW]
5100	60.75	1419.25
5400	65.19	1522.81
5600	97.62	2280.38
6000	46.34	1082.66
6100	96.30	2249.70

Table 6.7: A table showing how the import from the MTDC-grid were divided among the generators in the selected areas.

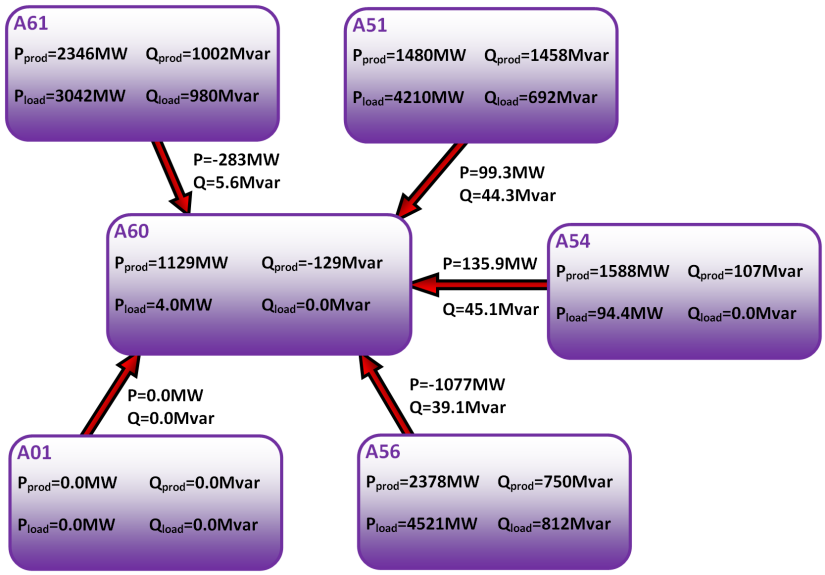

Figure 6.3: The power flow for the selected areas in the Nordic grid to be used as an initial condition in the dynamic simulations.

Chapter 7

Dynamic Simulations

This chapter will present the dynamic simulations performed to serve as a basis analyzes of the MTDC-grid operation.

7.1 The Simulated Scenarios

There were mainly four different questions to be answered by analyzing the dynamic behavior of the MTDC-grid.

1. Can the implemented control feature, with the Norwegian terminal operating as a DC-swingbus, assure a stable MTDC-grid operation?
2. How will the MTDC-grid operation effect the Nordic grid?
3. Will faults in one AC grid propagate through the MTDC-grid and disturb the operation of the others, and if so, to what degree?
4. What are the effects of applying AC-voltage control compared to reactive power control on the converter in Norway?

To answer these questions four simulation scenarios were chosen.

BaseCase – The Nordic grid model without the MTDC-grid connected. A direct three-phase to ground shortcircuit at node 5600 in the Nordic grid is applied. The fault is cleared after $70ms$ by disconnecting the transmission

line between node 5600 and 6000. The line is kept disconnected for the remaining simulated time.

Case1 – The complete model with the MTDC-grid connected to the Nordic grid model. The same fault scenario as for the BaseCase.

Case2 – An arbitrary fault resulting in loss of 350MW wind power production over a period of 100ms. Simulated by ramping the wind production from 700MW to 350MW in 100ms.

Case3 – A direct three-phase to ground short circuit at the offshore connection node BUS1_SNI. The fault is cleared after 70ms, and the 700MW of offshore wind production is maintained.

As specified in sec. 5.3.1, the converter station in Norway where implemented with two different sets of parameters for the DC-voltage regulation in order to see how the speed of the control feature would effect the MTDC-grid operation.

The Norwegian converter station was also tested with both reactive power control and AC-voltage control. The reactive power control where implemented to give a minimum supply of reactive power to the Nordic grid, giving the initial power flow presented in sec. 6.2. The AC-voltage control where implemented to keep the converter station node, BUS1_NO, equal to the value given by the power flow, 302.0kV. That way the initial condition for both control features where identical.

To study the effect of the different control features applied, and to see if and how they effect each other, the four sub-cases given in tab. 7.1 where performed for the different scenarios given above.

Sub-Case	Q-reg/AC-reg	DC-reg speed
A	Q-reg	Fast
B	Q-reg	Slow
C	AC-reg	Fast
D	AC-reg	Slow

Table 7.1: The table shows the different sub-cases performed. Reactive power control (Q-reg), AC-voltage control (AC-reg) and DC-voltage control (DC-reg)

7.2 The Dynamic Behavior of the Nordic Grid

The BaseCase scenario is simulated in order to see how the MTDC-grid operation effect the Nordic grid, by comparing it to the similar fault scenario in Case1. The initial condition of the grid was the unaltered power flow taken from [41]. However, as shown in fig. 7.1 the Nordic grid model was originally unstable.

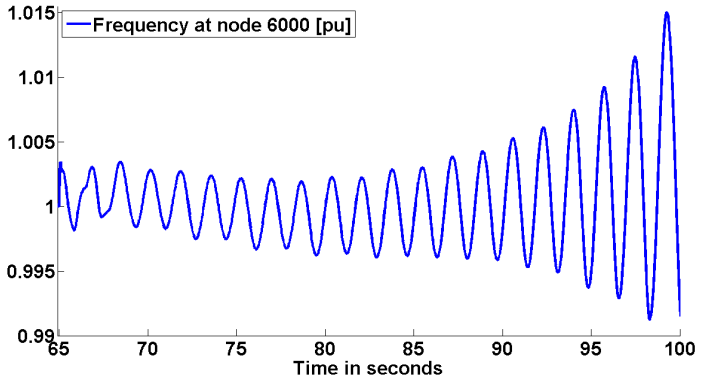

Figure 7.1: Frequency measurements on node 6000 for the unaltered Nordic grid model applied with a 3-phase fault on node 5600 at t=65.0s for 70ms followed by the disconnection of the transmission line between node 5600 and 6000.

To stabilize the model it where decided to add a power system stabilizer to the generator at node 5600, and increase the gain for the stabilizer for the generator on node 6100 [47]. With these alterations the system became stable, as shown in fig. 7.2.

Linear analysis were utilized to give the eigenvalues of the system. There where mainly three different complex eigenvalues, given in tab. 7.2, explaining the oscillations shown in the frequency response. In figure 7.2, the response explained by λ_3 is clearly shown as the oscillations damped in the course of three periods from t=80s to t=200s. The smaller more rapid oscillations visible in the time span from t=80s to t=120s is explained by λ_1. The oscillatory response corresponding to λ_2 is the dominating oscillations in the time span from t=65s to t=75s, shown in fig. 7.3.

It is evident from the frequency measurements and the presented eigenvalues

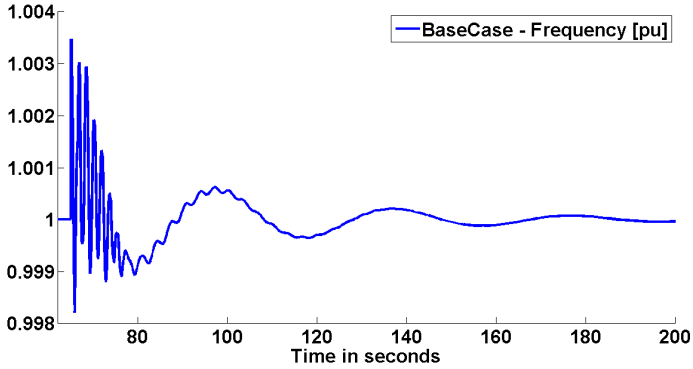

Figure 7.2: Frequency measurements on node 6000 for the Nordic grid model applied with additional power system stabilizer.

λ	α [1/s]	Ω [Hz]	ζ [s/s]	T_S [s]
1	-0.0596164	0.308827	0.189542	3.238
2	-0.376491	0.627764	0.514327	1.593
3	-0.0267519	0.0252723	0.726923	39.57

Table 7.2: The table shows the characteristic eigenvalues of the Nordic system. Presented are the real (α) and imaginary (Ω) part of the complex eigenvalues, their degree of damping (ζ) and time period (T_S).

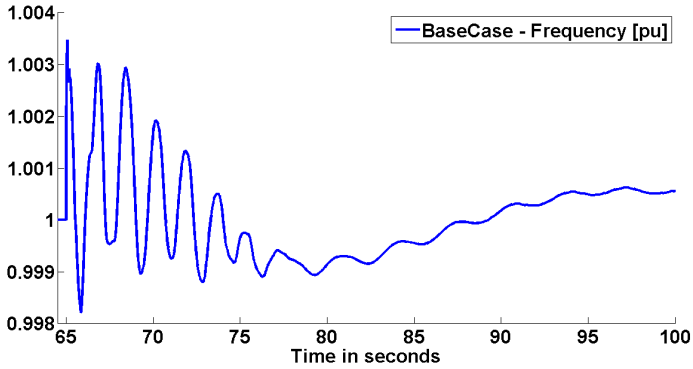

Figure 7.3: Frequency measurements on node 6000 for the Nordic grid model applied with additional power system stabilizer.

that the grid model is poorly damped, and hence not a realistic representation for the Nordic grid. However, attaining a model representing the dynamic responses of the Nordic grid was not a part of the scope for the thesis. It was therefore decided to use the Nordic grid model as it has been presented here. The model will still serve as a platform for studying the effect of the MTDC-grid operation. The influence of the MTDC-grid can be studied by comparing the responses with and without the MTDC-grid connected. However, it has to be noticed that the dynamic responses observed will not be a representation for the physical responses achieved, if the MTDC-grid presented were to be connected to the Nordic grid.

7.3 The Dynamic Simulations

For each simulation scenario an explanation of the cause and effect as the faults spread through the system will be highlighted. The results presented will primarily concern the MTDC-grid operation by studying the DC-voltages and power transfer. Measurements were also taken of the voltage at converter station terminals, BUS1_, and both active and reactive power supplied to each AC-grid. In the Nordic grid the analysis will concern the generator on the connection node 6000 as this is directly effected by the MTDC-grid. Active and reactive power production, speed, field- and terminal voltage of the generator are measured. A frequency measurement on the connection node 6000 is performed.

All the measured quantities for all the different scenarios studied will not be presented, but selected measurements showing the essential behavior will be given. The measurements from the different scenarios will be seperated by use of the names; BaseCase, Case1A,...,Case2C,...etc, followed by the name of the measured variable. All the measured quantities for the different scenarios are given in Appendix 11.

7.3.1 Case1

As the shortcircuit is applied it causes an instantaneous drop in the voltage at the connection node 6000. The voltage drop gives an initial reduction in the power drawn from the MTDC-grid as well as the electric torque in the generator at node 6000. A power surplus is experienced in the MTDC-grid charging the

DC-capacitors, resulting in a DC-voltage rise, as shown in fig. 7.4. As given

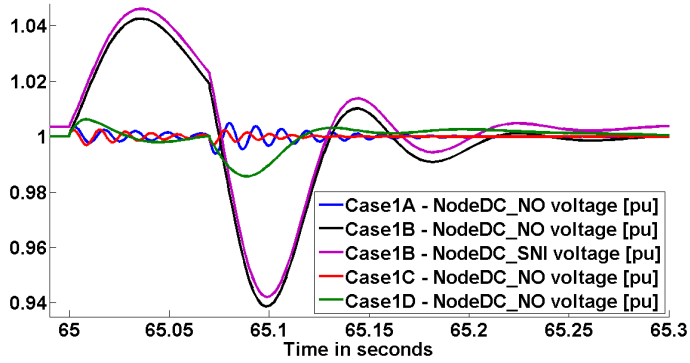

Figure 7.4: The figure shows the DC-voltage at the Norwegian converter station, DC_NO, for the four different sub-cases. Also shown in purple is the DC-voltage at node DC_SNI to illustrate how the whole MTDC-grid is effected.

by eq. (4.1), the power transfer in the MTDC-grid is directly linked to the difference in DC-voltage between to connected terminals. The initial increase in the DC-voltage at, DC_NO, will hence reduce the power transferred from the offshore converter terminal. This will again cause a power surplus at the terminal, DC_SNI, resulting in a voltage rise. Shown in fig. 7.4 is the DC voltage at DC_NO and DC_SNI for scenario, Case1B. It clearly shows how the voltage at DC_SNI follow the response at DC_NO, keeping the power transfer by a small voltage difference. Similar response is observed at the English converter station, implying that the whole MTDC-grid is oscillating.

However, as the deviations in voltage spread thought the MTDC-grid certain deviations in power transfer are experienced, affecting the import of active power for the English and offshore converter stations. The oscillations in power import are similar to that of the DC-voltage for the different sub-cases. The maximum deviation from the initial condition is given in tab. 7.3. As for the DC-voltage steady state operation, equal to the initial condition, is attained within 0.3s.

The oscillations in DC-voltage is linked to the deviation in power import for the Norwegian converter station, which is inflicted as it tries to restore a nominal voltage at the node DC_NO. The power import at the Norwegian terminal is given in fig. 7.5. It is evident that the speed of the DC-voltage regulation directly affect the frequency of the power oscillations. However, the amplitude

Converter Station:	Case1A	Case1B	Case1C	Case1D
SNI	26.86MW	55.85MW	3.45MW	31.15MW
	4.43%	9.22%	0.57%	5.14%
EN	1.5MW	14.8MW	0.75MW	2.75MW
	0.75%	7.4%	0.375%	1.38%

Table 7.3: The table shows the maximum deviation from the initial power flow, in [MW] and in percent of the initial power flow, for the offshore and English converter station.

for the power oscillations are quite similar in size as opposed to the difference experienced in DC-voltage.

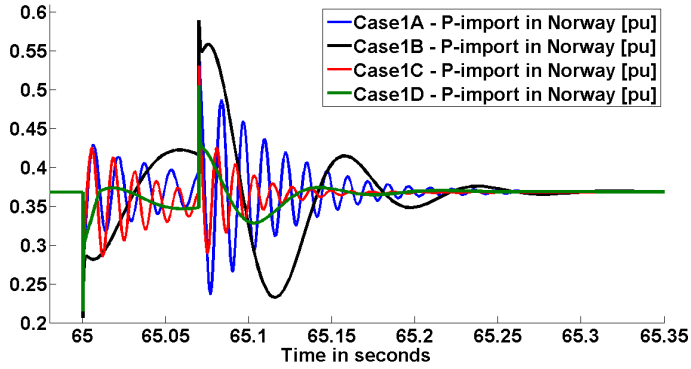

Figure 7.5: The figure shows the active power supplied by the Norwegian converter station, for the four different sub-cases.

Comparing Case1B with Case1D it is noticed that the AC-voltage control leads to reduced DC-voltage oscillations. Similar effect can also be seen for Case1A and Case1C. By studying the AC-voltage on the connection node 6000, fig. 7.6, it is evident that the AC-voltage control contributes to keeping a higher voltage both during and after the shortcircuit. This is accomplished as the full rating of the Norwegian converter is utilized to supply reactive power during the fault. The increased AC-voltage allows a higher power import as can be seen in fig. 7.5.

The main disturbance causing oscillations in the Nordic grid is the three-phase fault itself. As the power exchange with the MTDC-grid achieve a steady state, equal to the initial value, within 0.3s it was not expected that it would effect

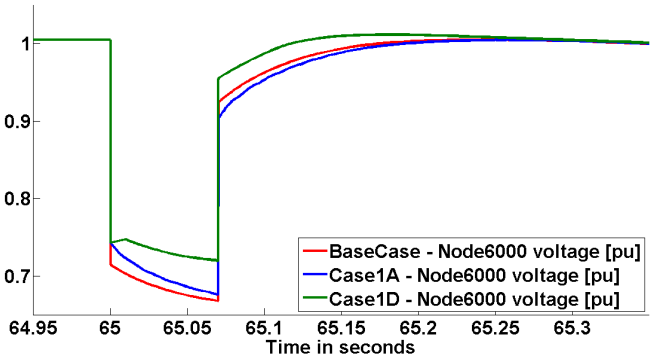

Figure 7.6: The figure shows the voltage at the connection node 6000 for the scenario simulated in BaseCase and Case1. Case1B and 1C is not shown as their responses are equal to 1A and 1D, respectively, implying that the speed of the DC-voltage regulation has no influence on the AC-voltage.

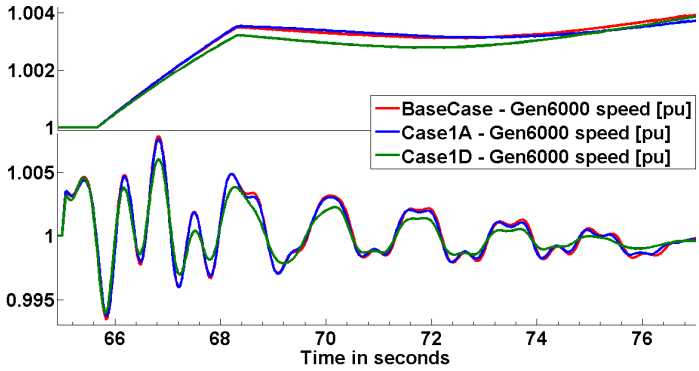

Figure 7.7: The figure shows the rotor speed of the generator connected to node 6000, the initial 0.3s are shown in the top graph. Case1B and 1C is not shown as their responses are equal to 1A and 1D, respectively, implying that the speed of the DC-voltage regulation has no influence on the generator speed.

the slow dynamic responses of the Nordic grid model to much degree. Given in fig. 7.7 is the rotor speed of the generator connected to node 6000. It shows how the loss of electric torque in the generator leads to an initial acceleration of the rotor. However, the increased AC-voltage achieved by applying AC-voltage regulation on the Norwegian converter station, does lead to an increased damping of the rotor speed oscillations in the first 10s after the fault. The same effect can be seen for the long frequency oscillations shown in fig. 7.8.

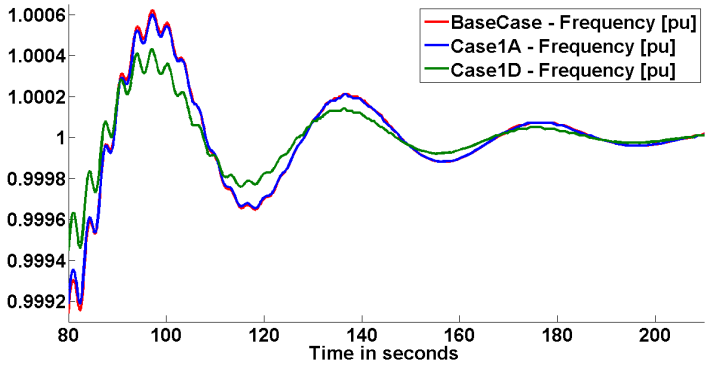

Figure 7.8: The figure show the frequency measured at node 6000. Case1B and 1C is not shown as their responses are equal to 1A and 1D, respectively, implying that the DC-voltage regulation has no influence.

7.3.2 Case2

In Case2 the offshore wind farm production is reduced from 700MW to 350MW in 0.1s. As the offshore converter station is operating as a AC-swingbus it compensates for the loss of wind production by reducing the export to the MTDC-grid. This imply a power deficit in the MTDC-grid resulting in discharge of the DC-capacitors giving a voltage drop at the node, DC_SNI. In figure 7.9 it clearly shown the difference of fast and slow DC-voltage regulation. For the fast regulation the voltage at DC_NO is kept constant as the Norwegian converter station is reducing it's power import according to the loss of wind production. The voltage at DC_SNI is reduced as the power transfer between the nodes decrease. For the slow DC voltage regulation the converter station in Norway does not respond as quickly and the DC-capacitors is discharged

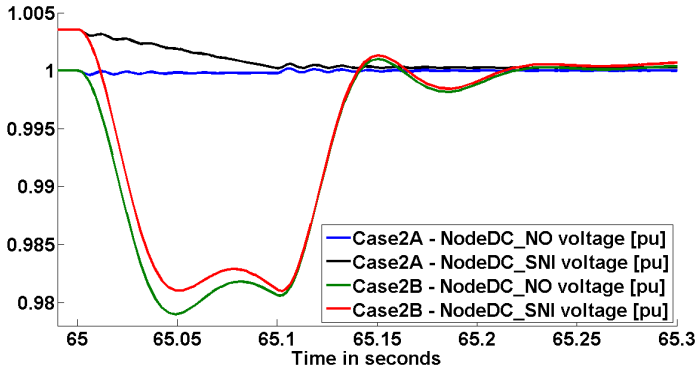

Figure 7.9: The figure show the DC-voltage on node DC_SNI and DC_NO for scenario Case2A and 2B. The scenarios 2C and 2D are not shown as they are equal to 2A and 2B, respectively, implying that the AC-voltage regulation has no influence.

giving a reduced voltage on the node DC_NO. Although, even with the slow DC-voltage regulation a stationary MTDC-grid operation is achieved within 0.3s.

As in Case1 the power import in the English converter station is effected by the deviations in DC-voltage, presented in tab. 7.4

Converter Station:	Case2A	Case2B	Case2C	Case2D
EN	0.2MW	3MW	0.2MW	3MW
	0.1%	1.5%	0.1%	1.5%

Table 7.4: The table shows the maximum deviation from the initial power flow, in [MW] and in percent of the initial power flow, for the English converter station.

The loss of wind production is almost directly transferred to the Nordic grid giving a deficit of 350MW which has to be compensated by the primary regulation. This causes an initial frequency drop of 0.175Hz followed by a overshoot of 0.05Hz before the oscillations is slowly damped, as shown in fig. 7.10. The figure show that neither the speed of DC-voltage regulation or applying AC-voltage regulation has any considerable effect on the oscillations. As shown in figure 7.11 the AC-voltage control is able to keep a stable voltage, equal to the reference, at the converter station terminal, BUS1_NO. Although, as the volt-

age deviations in scenario, Case2A, only has minor deviations less than 0.9kV the effect of applying the AC-voltage control is minimal.

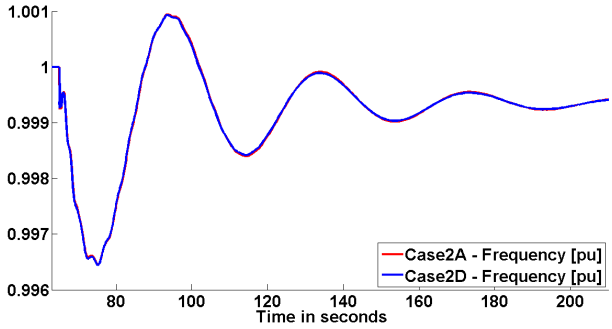

Figure 7.10: The figure show the frequency measured at node 6000, for scenario Case2A and Case2D. The result for all four sub-cases where equal, implying that neither the speed of DC-voltage regulation or AC-voltage regulation has any effect on the oscillations.

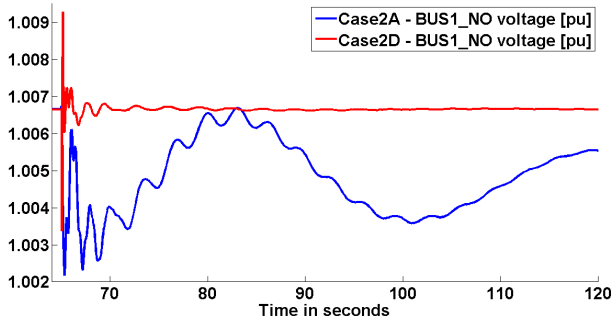

Figure 7.11: The figure show the voltage at the Norwegian converter station terminal, BUS_NO.

7.3.3 Case3

Shown in the top graph of figure 7.12 is how the three-phase fault at BUS1_SNI causes the power export of the offshore converter station to drop to zero, im-

plying a instantaneous loss of 700MW. Only after the fault is cleared are the power export restored over a period of 0.2s.

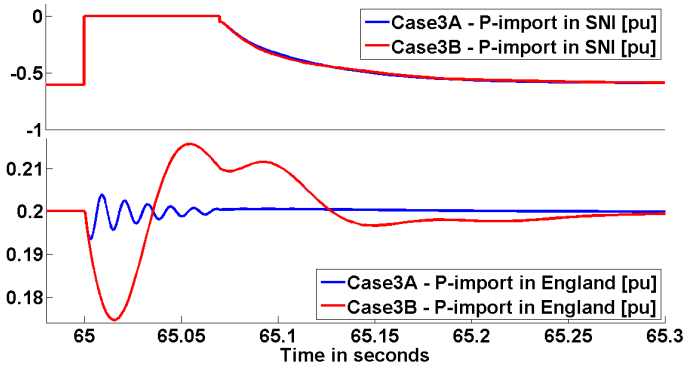

Figure 7.12: The figure show the power import at the offshore converter station (top graph) and English converter station (bottom graph) for simulation scenario Case3.

The power deficit in the MTDC-grid imply a reduction in the DC-voltage as shown in fig. 7.13. Compared to both Case1 and Case2 this result in more severe initial decrease of the DC-voltage, and corresponding oscillations. However, before the fault is cleared at t=65.07, have both the slow and fast DC-voltage regulation been able to restore the DC-voltage. As the fault is cleared a voltage surge is observed as the power export from the offshore converter station is restored.

The corresponding power import in the English converter station, fig. 7.12, show that a deviation from the initial power flow of 12.8% and 3.25% for the slow and fast DC-voltage regulation, respectively.

As for the two previously shown scenarios it is the Norwegian converter station, implemented with DC-voltage regulation, that has to balance the power deficit due to the fault. This imply that the Norwegian converter station has to go from importing 368MW to exporting the 200MW imported at the English terminal in additional to losses in the MTDC-grid. Figure 7.14 show that both the fast and slow DC-voltage regulation inflict this deficit onto the Nordic grid, with the largest deviation close to 1100MW from the initial condition for the fast regulation. However, evident in fig. 7.14 is that the initial power import of 368MW is restored within a short time frame of 0.3s.

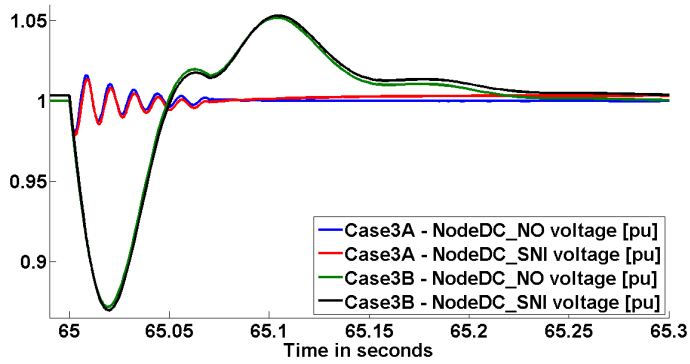

Figure 7.13: The figure show the DC-voltage at the nodes, DC_NO and DC_SNI, for both Case3A and Case3B.

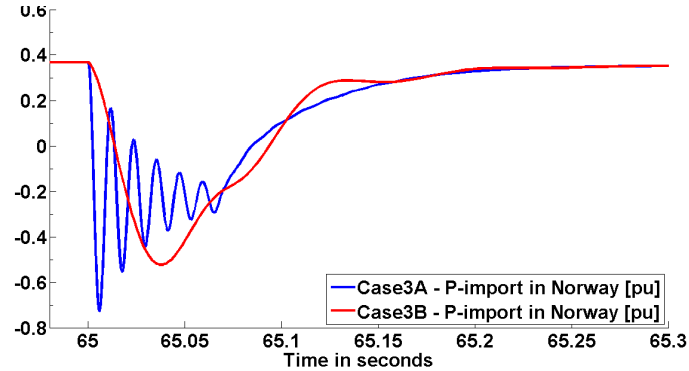

Figure 7.14: The figure show the power imported at the Norwegian converter station, for both Case3A and Case3B.

Even though a high power deviation is inflicted, the fast recovery of initial conditions result in only minor oscillations in the measured frequency and generator speed.

Chapter 8

Discussion

The investigation of the MTDC-grid operation has shown that a limited export, of 215MW, from the English grid is attainable during maximum production from the offshore wind farm. This is because the Norwegian terminal is brought to it's current limit. As there are many wind farms planned at the coast of England it is expected that during high wind situations there is a desire to export power. A solution would be to increase the rating of the Norwegian converter station. As a suggestion, increasing the rating by 100MVA would imply a 50% increase in power export from the English terminal during maximum wind production. This increase would also be usefull in a situation with no offshore wind production, as the Norwegian converter station would be capable of supplying the offshore oil and gas installations as well as full power import of the English terminal.

It was also noticed that the power exchange with England was limited by low voltage at the AC-side of the converter station. As stated, the low voltage was caused by an unfavorable transfer of reactive power combined with voltage drop in the transmission line connecting the converter to the node representing the English grid. This emphasizes, that with the level of power exchange intended, theses converter stations need a suitable grid connection. The low voltage could be compensated by use of the reactive power control on the converter station, adjusting the reference value for certain changes in power flow. Another possibility would be to apply AC-voltage control instead, which would give a constant adjustment of the reactive power supplied. The converter control could also be combined with a tap-changer on the converter transformer, adjusting the volt-

age ratio according to the degree of power exchange. However, due to time limitations no such investigations were performed.

Transmission and converter losses were calculated, resulting in a total loss for the MTDC-grid in the range of 5-7% of supplied power. However, these percentages are under maximum loading scenarios. As the converters consist of a considerable amount of no-load losses, $\approx 10MW/converter$, an increasing loss percentage will be experienced as the loading decrease. It has to be noticed that an overestimation has been done when implementing the converter losses, thus, it should be viewed as such. Espechially as the converter losses make up about 3/4'th of the total losses in the MTDC-grid.

Considering the dynamic simulations it was desirable to see if the implemented control feature could assure a stable MTDC-grid operation. The simulations show that both the slow and fast DC-voltage regulation achieved a stationary conditions within 0.3s of any disturbance applied. After this stabilizing period the DC-voltage and hence the power flow in the MTDC-grid were kept constant even though considerable perturbations where measured in the connected Nordic grid model.

The tuning of the regulation, implemented on each converter, where performed on a simplified model. This was due to a challenging implementation of the full model utilized for the simulations, which were only completed in time to perform the simulations shown. Therefore, two different sets of parameters for the DC-voltage regulation were chosen in order to study their effect. As the simulations show both the slow and fast regulation gave an oscillatory response to disturbances, contributing to unnecessary large fluctuations in power exchange with the Nordic grid. Further investigations of the parameterization of the converter regulation could lead to an optimization of inflicted power fluctuations in the Nordic grid, compared to DC-voltage oscillations in the MTDC-grid.

Non the less, the fast dynamic response of the MTDC-grid is dominated by the size of the DC-capacitors, giving the degree of voltage deviation according to power deficit or surplus in the grid. Therefore, any change in power exchange will have to be compensated by the converter operating as the DC-swingbus within a short time frame in order to prevent large deviations in DC-voltage. As shown by the simulations this will imply that the AC-grid designated to balance the MTDC-grid has to have the capability to withstand any disturbances that can be inflicted by the MTDC-grid. A relative severe fault in the offshore AC grid, Case3, did only lead to minor disturbances in the Nordic grid. The reason for this was that the pre-fault condition were restored quickly after the fault

was cleared. This emphasizes the advantage of fault ride through capabilities for the wind farms connected in the offshore AC grid.

However, faults that rendered a whole converter station out of service could occur, and for the implemented control structure a worst case scenario would be if the Norwegian converter station were disconnected. In such a case the MTDC-grid would have no means of regulation. As discussed in Chapter 4 control structures like marginal or droop control could be applied, which would have means to cope with such a situations.

Chapter 9

Conclusion and Further Work

This thesis has investigated the operation of a three-terminal DC-grid. The DC-grid considered, was a proposed structure interconnecting the two countries Norway and England with an offshore terminal connected midway, allowing integration of an offshore wind farm and oil platform. Firstly, theory and technological development for HVDC-VSCs as well as control features for operating a MTDC-grid has been reviewed to serve as a basis for model implementation and analyzes performed. A model of the DC-grid has been built in the simulation tool SIMPOW, and further connected to a 35-node AC-grid model, in order to study the steady state limitations as well as dynamic behavior of the complete structure.

Power flow calculations performed showed that the DC-grid could allow for a power exchange with only 5-7% loss during different maximum load scenarios. There was experienced limitation in power export for the English terminal during high wind situations, due to equal rating of the three terminals. It is suggested to increase the Norwegain terminal rating by 100MVA allowing for a 50% increase in the English power export. This would also allow for rated power import for the English terminal during zero wind production.

The DC-grid operation during a series of disturbances where studied with the Norwegian terminal equipped with DC-voltage control. Following a disturbance

a power deficit or surplus would be experienced in the DC-grid. In the event of a power deficit, the DC-capacitors would be discharged and lead to a decreasing voltage, and a surplus would lead to charging followed by an increasing voltage. The control feature of the Norwegian terminal would compensate for this by adjusting it's power exchange. As the dynamics of the DC-capacitors are in the range of *m*s, it implies that a fast response of the DC-voltage control is needed to avoid unnecessary low or high voltages.

The simulations performed showed that a stable DC-grid operation were attained within no more than 0.3s of the applied faults. As a consequence any power unbalance inflicted to the DC-grid were directly transferred to the Nordic grid. This implies that the Nordic grid has to have the capability to handle any disturbance possible to be inflicted by the DC-grid. The benefit of fault ride through capability of the offshore wind farm was emphasized, as it will diminish the power unbalance inflicted onto the Nordic grid following a fault.

The influence of the power transfer to both the English and Offshore AC grid were noticed to be directly linked to the DC-voltage fluctuations. The deviation from the desired power exchange ranged from 0.375% to 12.8% for the different fault scenarios and regulation alternatives. In the perspective of the severe faults that were applied, this is seen as accepeble influence, espechially, due to the short time period of the deviation. Although, it further identifies the need for a fast and accurate DC-voltage regulation.

A comparison of AC-voltage control and reactive power control for the Norwegian converter station was performed. It showed that the AC-voltage control utilized the full converter rating for supply of reactive power during a three-phase to ground fault in the Nordic grid model. This contributed to a higher voltage at the MTDC-grid connection point during and after the fault, giving an enhanced capability for power exchange and thereby reduced DC-voltage oscillations. The control action also contributed to increased damping of the rotor speed oscillations for the generators close to the connection point, implying an enhanced stability for the connected AC-grid.

9.0.4 Further Work

The model implementation and simulations performed has identified key aspects of the dynamic operation of the three-terminal DC-grid, but are in no means a complete analysis of the structure. Further investigations and model implemen-

tations are needed to fully identify the grid operational limits and demand for control features.

The DC-grid control feature analyzed was with the Norwegian converter station operating as the balancing unit for the DC-grid. It has shown to give a fast response able to balance the DC-grid for sever faults. However, the control gave an response with unnecessary large power oscillations inflicted in the connected AC-grid. Further investigations into regulator tuning is needed to get an optimal response as a balance between DC-voltage deviations and power oscillations inflicted.

As the control feature analyzed operated with only one balancing unit for the DC-grid. A fault bringing the converter station to it's limits or even worse disconnecting it, will render the DC-grid uncontrolled and most likely a total collapse of the grid operation. Therefore, implementation and further investigations of control features like voltage margin or voltage droop control is needed.

Not analyzed in this thesis, is how faults in the DC-grid itself will be handled. Investigations of DC-fault detection and clearing schemes has to be performed. System analysis can be utilized to identify the critical clearing time and duration of DC-grid disconnection following a fault. The duration of disconnection will have to be weighted against implementation of expensive DC-breaker components.

List of Figures

List of Tables

Bibliography

[1] Dr. Nicolas Fichaux and Justin Wilkes. Oceans of Opportunity – Harnessing Europe's largest domestic energy resource. Technical report, EWEA, September 2009.

[2] European Commission's official page for climate change. `http://ec.europa.eu/environment/climat/home_en.htm`.

[3] Nils Martin Espegren and at all. *Havvind – Forslag til utredningområder*. Fladby Grafisk AS, Oktober 2010.

[4] Krzysztof Rudion, Hans Abilgaard, Antje G. Orths, and Zbigniew A. Styczynski. Analysis of Operational Strategies for Multi-Terminal VSC HVDC Systems. Oct. 2010. 9th International Workshop on Large-Scale Intergration of Wind Power as well as on Transmissin Systems for Offshore Power Plants. Québec, Canada.

[5] Thomas Tr'oscher and Magnus Korpås. Optimal Design of a Subsea Power Grid in the North Sea. September. Eurpean Offshore Wind Conference (EOW'09), Stockholm.

[6] Bengt Johansson. System Analysis South North Sea. Technical Report 2011008-06-0.3, Solvina, July 2011.

[7] ABB Reference project. The early HVDC development. `http://www05.abb.com/global/scot/scot221.nsf/veritydisplay/8cf1c44dbc522685c12574e9006051a5/\$File/The\%20early\%20HVDC\%20development.pdf`.

[8] Xiangjiaba - Shanghai UHVDC transmission project. `http://www.abb.com/industries/ap/db0003db004333/148bff3c00705c5ac125774900517d9d.aspx`.

[9] Riccardo Bodega. *Space Charge Accumilation in Polymeric High Voltage DC Cable Systems*. PhD thesis, Delft University of Technology, 2006.

[10] Abb's official webpage for HVDC. `http://www.abb.com/hvdc`.

[11] N. Mohan, T. M. Undeland, and W.P. Robbins. *Power Electronics Converters, Application and Design*. Wiley, 2003.

[12] Nikolas Flourentzou, Vassilios G. Agelidis, and Georgios D. Demetriades. VSC-Based HVDC Power Transmission Systems: An Overview. *IEEE Transactions on Power Electronics*, 24(3), 2009.

[13] Trans Bay Cable Project, in California USA. `http://www.energy.siemens.com/us/en/power-transmission/hvdc/hvdc-plus/references.htm`.

[14] N. M. MacLeod, A. C. Lancaster, and C. D. M. Oates. The development of a Power Electronic Building Block for use in Voltage Source Converters for HVDC transmission applications. Technical Report 402 B4, Cigré SC, 2009.

[15] Bjorn Jacobson, Patrik Karlsson, Gunnar Asplund, Lennart Harnefors, and Tomas Jonsson. VSC-HVDC Transmission with Cascaded Two-Level Converters. Technical Report 110 B4, Cigré, 2010.

[16] Hartmut Huang. Multilevel Voltage-Sourced Converters for HVDC and FACTS Applications. Technical Report 401 B4, Cigré SC, 2009.

[17] Rohitha P. Jayasinghe Udana N. Gnanarathna, Aniruddha M. Gole. Efficient Modeling of Modular Multilevel HVDC Converters (MMC) on Electromagnetic Transient Simulation Programs. *IEEE Transactions on Power Delivery*, 26(1), 2011.

[18] Chandra Bajracharya. Control of VSC-HVDC for Wind Power. Master's thesis, The Norwegian University of Science and Technology, 2008.

[19] J. Reeve. Multiterminal HVDC Power Systems. *IEEE Transactions on Power Apparatus and Systems*, 99(2), 1980.

[20] W. F. Long, J. Reeve, J. R. McNichol, M. S. Holland, J. P. Taisne, J. LeMay, and D. J. Lorden. Application Aspects of Multiterminal DC Power Transmission. *IEEE Transactions on Power Delivery*, 5(4), 1990.

[21] ABB Reference project. The HVDC Transmission Québec–New England. `http://www.abb.no/industries/ap/db0003db004333/87f88a41a0be97afc125774b003e6109.aspx`.

[22] Temesgen M. Haileselassie, Tore M. Undeland, and Kjetil Uhlen. Multiterminal HVDC for Offshore Windfarms – Control Strategy. May 2011. EPE Joint Wind Energy and T&D Chapters Seminar.

[23] Grain P. Adam, Olimpo Anaya-Lara, and Graeme Burt. Multi-terminal dc transmission system based on modular multilevel converter. September 2009. 44th International Universities Power Engineering Conference (UPEC).

[24] Servando González-Hernández, Edgar Moreno-Goytia andFernándo Martinez-Cardenas, and O. Anaya-Lara. Analysis of Integrated Wind Farm Using a Multiterminal VSC-HVDC: Different Electrical Conditions Response. September 2008. 40th North American Power Symposium.

[25] Lianxiang Tang and Boon-Teck Ooi. Locating and Isolating DC Faults in Multi-Terminal DC Systems. *IEEE Transactions on Power Delivery*, 22(3), 2007.

[26] Christian M. Franck. HVDC Circuit Breakers: A Review Identifying Future Research Needs. *IEEE Transactions on Power Delivery*, 26(2), 2011.

[27] Carl Öhlén, Math Bollen, and Max Degerfält. Offshore grid – Fault detection. Technical Report R09-617, STRI, Desember 2009.

[28] Lianxiang Tang and Boon-Teck Ooi. Protection of VSC-Multi-Terminal HVDC against DC Faults. 2002. Power Electronics Specialists Conference, IEEE 33rd Annual.

[29] T. Nakajimaand and S. Irokawa. A Control System for HVDC Transmission by Voltage Sourced Converters. 1999. Power Engineering Society Summer Meeting, IEEE.

[30] Jan Machowski, Janusz W. Bialek, and James R. Bumby. *Power System Dynamics – Stability and Control*, pages 335–341. Wiley, 2nd edition, 2009.

[31] B.K. Johnson, R.H. Lasseter, F.L. Alvarado, and R. Adapa. Expandable Multiterminal DC Systems Based on Voltage Droop. *IEEE Transactions on Power Delivery*, 8(4), 1993.

[32] Temesgen Mulugeta Haileselassie. Control of Multi-terminal HVDC-VSC Systems. Master's thesis, The Norwegian University of Science and Technology, 2008.

[33] Gustavo Pinares Ccorimanya. Opeation of HVDC Grids in Parallel with AC Grids. Master's thesis, Chalmers University of Technology, 2010.

[34] STRI AB. *Simpow Manual – Power System Simulation Software*, 11.0 edition, 2008.

[35] STRI AB. *Simpow Manual – Power System Simulation Software*, 11.0 edition, 2008. Chap. 25.

[36] Matias Ebbe Theisen. Offshore Grid. Technical report, NTNU, Desember 2010.

[37] SINTEF Energy Research. `http://http://www.sintef.no/`.

[38] Bjørn Harald Bakken. *Technical and Economical Aspects of Operation of Thermal and Hydro Power Systems*. PhD thesis, Norwegian University of Science and Technology, 1997.

[39] Kjetil Uhlen, Ian Norheim, Elin Lindgren, Sanna Uski, Poul Sørensen, and Clemens Jauch. D5.1 – System Stability Analysis. Technical report, WILMAR, September 2005. Available at: `http://www.wilmar.risoe.dk`.

[40] Guillaume Verez. System Integration of Large Scale Offshore Wind Power. Master's thesis, Norwegian University of Science and Technology, 2011.

[41] Bjørn Harald Bakken. Dynamisk modell for studier av primær- og sekundærregularing i Norge. Technical report, EFI – Sintef Gruppen, November 1997. AN-97.12.22 (Only Norwegian).

[42] Bjørn Harald Bakken. Aktive reserver – Beregningseksempel Lastflytanalyser. Technical report, EFI – Sintef Gruppen, June 1997. AN-97.12.09 (Only Norwegian).

[43] Jan Machowski, Janusz W. Bialek, and James R. Bumby. *Power System Dynamics – Stability and Control*. Wiley, 2nd edition, 2009.

[44] STRI AB. *Simpow Manual – Power System Simulation Software*, 11.0 edition, 2008. Chap. 20.

[45] STRI AB. *Simpow Manual – Power System Simulation Software*, 11.0 edition, 2008. Chap. 14.2.16.

[46] STRI AB. *Simpow Manual – Power System Simulation Software*, 11.0 edition, 2008. Chap. 20.4.

[47] Consultation and discusstions with Prof. Kjetil Uhlen at NTNU.

[48] STRI AB. *Simpow Manual – Power System Simulation Software*, 11.0 edition, 2008. Chap. 22.

Chapter 10

Model Parameters

In this Appendix the different model parameters are presented.

10.1 Oil Platform

Connection nodes	SN [MVA]	UN1 [kV]	UN2 [kV]	R [pu]	X [pu]
BUS21 PB21	100	132	13.8	0.005	0.10
PB21 PB212	5	13.8	6.0	0.008	0.08
PB21 PB212	12	13.8	6.0	0.006	0.09

Table 10.1: Oil platform transformer values

Node 1	Node 2	L [km]	R [Ω/km]	X [Ω/km]	B [$\Omega^{(} - 1$)/km]
BUS2_SNI	BUS21	10	0.07	0.07	0.000107
PB21	PB211	0.300	0.125	0.132	0.000106
PB21	PB214	0.15	0.125	0.132	0.000106
BUS2_SNI	BUS2T	1	0.07	0.07	0.000107

Table 10.2: Oil platform cable parameters

10.2 Nordic Grid

All the model parameters for the Nordic grid is given the optpow- and dynpow-files in Appendix 11. Table 10.3 present the explanation for each parameter given for the generator models in the dynpow-file given in Appendix 11.

Parameter	Description
SN	Power rating in [MVA]
UN	Rated voltage in [kV]
H	Inertia constant in [MWs/MVA]
D	Damping constant in [pu torque/pu speed]
RA	Stator winding resistance [pu]
XA	Stator leakage reactance [pu]
XD	D-axis synchronous reactance [pu]
XDP	D-axis transient reactance[pu]
XDB	D-axis subtransient reactance[pu]
TD0P	D-axis transient open-circuit time constant in [s]
TD0B	D-axis subtransient open-circuit time constant in [s]
XQ	Q-axis synchronous reactance [pu]
XQP	Q-axis transient reactance[pu]
XQB	Q-axis subtransient reactance[pu]
TQ0P	Q-axis transient open-circuit time constant in [s]
TQ0B	Q-axis subtransient open-circuit time constant in [s]
V1	D-axis subtransient reactance[pu]
V2	D-axis synchronous reactance [pu]
SE1	D-axis transient reactance[pu]
SE2	D-axis subtransient reactance[pu]

Table 10.3: Input parameters for the round-rotor generator model.

10.3 Three-terminal DC grid and Converters

The parameters given below for transformer, AC-filter and DC cables are based on a model of ABB's HVDClight converter in the SIMPOW manual [48], given in Appendix 11. The values presented are calculated by use of interpolation

according to MVA rating of the converter. The interpolation has been done between the values given for M8 and M9, as presented in eq. (10.1).

$$X_{used} = X_{M9} + (X_{M8} - X_{M9}) \frac{1000 - S_{M9,rating}}{S_{M8,rating} - S_{M9,rating}} \tag{10.1}$$

As the filter and transformer had to switch places the filter comonents where scaled according to eq. (10.2)

$$Z_{secondary} = n^2 \, Z_{primary} \tag{10.2}$$

where n is the turn ratio of the transformer and Z is the impedance value.

With these calculations the following model parameters were implemented.

Station	SN [MVA]	UN1 [kV]	UN2 [kV]	R [pu]	X [pu]
Norway	1059	400	300	0.0	0.12
Offshore	1059	400	132	0.0	0.12
England	1059	400	300	0.0	0.12

Table 10.4: Converter station transformer values

Station	XC [Ω]	XS [Ω]
Norway	-600.000	15.96
Offshore	-116.160	3.708
England	-600.000	15.96

Table 10.5: Converter station AC-filter values

Node 1	Node 2	L [km]	R [Ω/km]	C/2 [μF]
DC_NO	DC_SNI	3.0	1.278	24.96
DC_SNI	DC_EN	3.5	1.278	34.95

Table 10.6: DC-cable resistance and shunt capacitance

10.3.1 Regulator Step Response

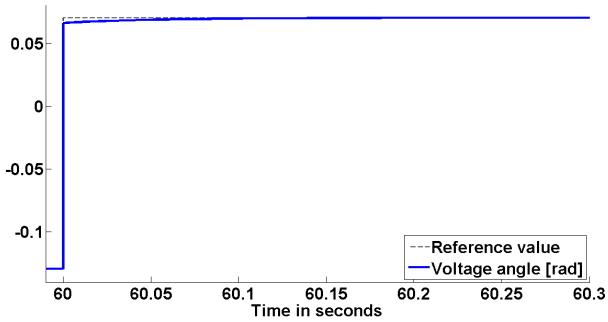

Figure 10.1: Phase regulator step response.

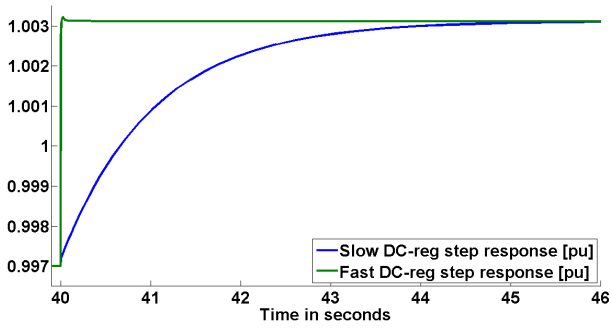

Figure 10.2: DC voltage regulator step response.

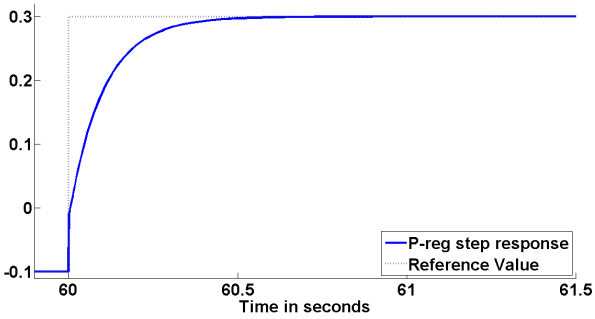

Figure 10.3: Active power regulator step response.

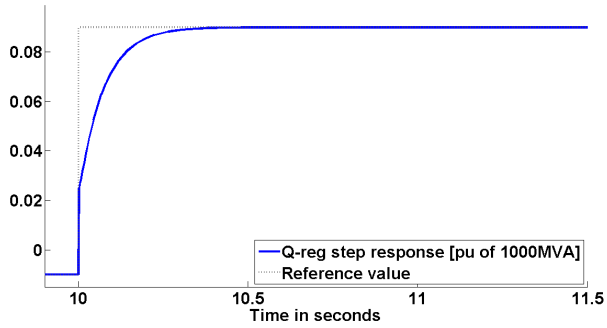

Figure 10.4: Reactive power regulator step response.

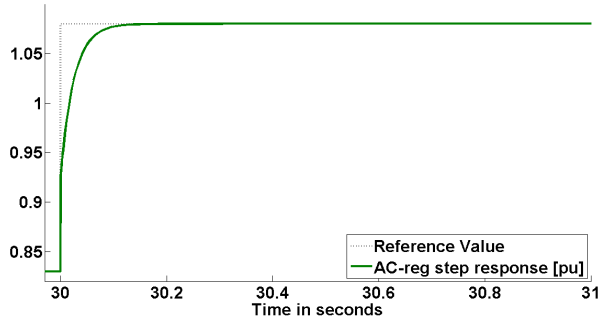

Figure 10.5: AC voltage regulator step response.

Chapter 11

SIMPOW-files

Here the simulation files contained in OffshoreGrid.zip is presented.

ConverterTEST.optpow the system topology for tuning of converter regulation, shown is the implementation for active and reactive power control.

BaseCase.optpow the system topology and power flow description for the simulation scenario BaseCase taken from [40].

Qreg.optpow the system topology and power flow description for all simulation scenarios with reactive power control implemented at the Norwegian terminal.

ACreg.optpow the system topology and power flow description for all simulation scenarios with AC-voltage control implemented at the Norwegian terminal.

ConverterTEST.dynpow input data for tuning of converter regulation, shown is the implementation for active and reactive power control.

BaseCase.dynpow the input data for dynamic behavior for the simulation scenario BaseCase taken from [40].

Qreg.dynpow the input data for dynamic behavior for all simulation scenarios with reactive power control implemented at the Norwegian terminal.

ACreg.dynpow the input data for dynamic behavior for all simulation scenarios with AC-voltage control implemented at the Norwegian terminal.

Graphs folder containing the simulation results in .fig and .xlsx format.

Simpow-11.pdf the SIMPOW manual